ผลเฉลยเชิงวิเคราะห์ของหน่วยแรงทีสำหรับรอยร้าวรูปวงกลม
ในตัวกลางยืดหยุ่นเชิงเส้นที่มีคุณสมบัติเหมือนกันตามขวาง 3 มิติ

ว่าที่ร้อยตรีมัฒนะ พินิจพานิชย์

วิทยานิพนธ์นี้เป็นส่วนหนึ่งของการศึกษาตามหลักสูตรปริญญาวิศวกรรมศาสตรมหาบัณฑิต
สาขาวิชาวิศวกรรมโยธา ภาควิชาวิศวกรรมโยธา
คณะวิศวกรรมศาสตร์ จุฬาลงกรณ์มหาวิทยาลัย
ปีการศึกษา 2556

ANALYTICAL SOLUTION OF T-STRESS FOR PENNY-SHAPED CRACK IN 3D TRANSVERSELY ISOTROPIC LINEAR ELASTIC MEDIUM

Acting Sub Lieutenant Matana Pinitpanich

A Thesis Submitted in Partial Fulfillment of the Requirements
for the Degree of Master of Engineering Program in Civil Engineering
Department of Civil Engineering
Faculty of Engineering
Chulalongkorn University
Academic Year 2013

Thesis Title	ANALYTICAL SOLUTION OF T-STRESS FOR PENNY-SHAPED CRACK IN 3D TRANSVERSELY ISOTROPIC LINEAR ELASTIC MEDIUM
By	Acting Sub Lieutenant Matana Pinitpanich
Field of Study	Civil Engineering
Thesis Advisor	Associate Professor Jaroon Rungamornrat, Ph.D.

Accepted by the Faculty of Engineering, Chulalongkorn University in Partial Fulfillment of the Requirements for the Master's Degree

.....Dean of the Faculty of Engineering

(Professor Bundhit Eua-arporn, Ph.D.)

THESIS COMMITTEE

.....Chairman

(Professor Teerapong Senjuntichai, Ph.D.)

.....Thesis Advisor

(Associate Professor Jaroon Rungamornrat, Ph.D.)

.....Examiner

(Associate Professor Akhrawat Lenwari, Ph.D.)

.....External Examiner

(Weeraporn Phongtinnaboot, Ph.D.)

มัฒนะ พินิจพานิชย์ : ผลเฉลยเชิงวิเคราะห์ของหน่วยแรงทีสำหรับรอยร้าวรูปวงกลมในตัวกลางยืดหยุ่นเชิงเส้นที่มีคุณสมบัติเหมือนกันตามขวาง 3 มิติ. (ANALYTICAL SOLUTION OF T-STRESS FOR PENNY-SHAPED CRACK IN 3D TRANSVERSELY ISOTROPIC LINEAR ELASTIC MEDIUM) อ.ที่ปรึกษาวิทยานิพนธ์หลัก: รศ. ดร. จรูญ รุ่งอมรรัตน์, 47 หน้า.

วิทยานิพนธ์ฉบับนี้นำเสนอผลเฉลยเชิงวิเคราะห์ของหน่วยแรงทีสำหรับรอยร้าวรูปวงกลมในตัวกลางยืดหยุ่นเชิงเส้นที่มีคุณสมบัติเหมือนกันตามขวางภายใต้แรงกระทำแบบผสมทั่วไป สนามหน่วยแรงสำหรับแรงกระทำพื้นฐานสองประเภทคือแรงคู่ขนาดหนึ่งหน่วยทิศทางตรงข้ามกันกระทำในแนวตั้งฉากและแรงคู่ขนาดหนึ่งหน่วยทิศทางตรงข้ามกันกระทำในแนวสัมผัสกับแต่ละพื้นผิวของรอยร้าวคำนวณได้จากทฤษฎีฟังก์ชันศักย์ จากนั้นดำเนินการหาค่าลิมิตของสนามหน่วยแรงดังกล่าวอย่างเหมาะสมเพื่อให้ได้ฟังก์ชันกรีนของหน่วยแรงทีในรูปแบบปิด จากนั้นประยุกต์ใช้หลักการรวมแบบเชิงเส้น ทำให้สามารถหาหน่วยแรงทีสำหรับรอยร้าวรูปวงกลมภายใต้แรงกระทำคู่สมดุลทั่วไปในรูปของสูตรเชิงปริพันธ์ ผลเฉลยเชิงตัวเลขสำหรับแรงกระทำบางประเภทได้นำมาเปรียบเทียบกับผลเฉลยอ้างอิงเพื่อยืนยันความถูกต้องของวิธีการและผลเฉลยที่นำเสนอ สุดท้ายทำการศึกษาอิทธิพลของสภาพแรงกระทำและคุณสมบัติของวัสดุตัวกลางที่มีต่อหน่วยแรงที

ภาควิชา วิศวกรรมโยธา ลายมือชื่อนิสิต .....

สาขาวิชา วิศวกรรมโยธา ลายมือชื่อ อ.ที่ปรึกษาวิทยานิพนธ์หลัก .....

ปีการศึกษา 2556

5570335621 : MAJOR CIVIL ENGINEERING
KEYWORDS: T-STRESS / GREEN'S FUNCTION / PENNY-SHAPED CRACK / MIXED-MODE LOADING / TRANSVERSELY ISOTROPIC ELASTIC MEDIA

MATANA PINITPANICH: ANALYTICAL SOLUTION OF T-STRESS FOR PENNY-SHAPED CRACK IN 3D TRANSVERSELY ISOTROPIC LINEAR ELASTIC MEDIUM. ADVISOR: ASSOC. PROF. JAROON RUNGAMORNRAT, Ph.D., 47 pp.

This thesis presents an analytical solution of the T-stresses for a penny-shaped crack in a transversely isotropic, linearly elastic infinite medium under general mixed-mode loadings. A complete stress field for two fundamental loading conditions associated with a pair of self-equilibrated unit normal and tangential point forces acting on both crack surfaces is obtained first via a technique of potential theory. Such explicit solutions are then utilized along with the proper limiting process to derive closed-form Green's functions for the T-stresses. By using a method of superposition, the T-stresses of a penny-shaped crack subjected to general self-equilibrated tractions on the crack surface can be obtained explicitly in terms of an integral formula. Numerical results for some special loading conditions are then compared with available benchmark solutions to verify the formulation and derived solutions. Finally, influence of loading conditions and material properties will be investigated and discussed.

Department: Civil Engineering Student's Signature .....
Field of Study: Civil Engineering Advisor's Signature .....
Academic Year: 2013

ACKNOWLEDGEMENTS

I would like to thank my advisor, Associate Professor Dr. Jaroon Rungamornrat, who always provides constructive and useful comments for the entire course of this investigation. I would also like to thank the Department of Civil Engineering, Chulalongkorn University for providing me the good opportunity to pursue my graduate study and also supporting me for any requirement to complete this thesis. I would like to express my sincere thanks to my parents and family who always encourage and support me and to my friends and everyone who helps me to complete this work.

CONTENTS

Page

Page

LIST OF TABLES

Page

LIST OF FIGURES

Page

Page

CHAPTER I
INTRODUCTION

1.1 General

Pre-existing flaws and load-induced damages present within engineering and industrial designed components and parts have been found the major cause of failures and loss of their original functions. Initial small defects and damages can act as both a localized stress riser and a global strength reducer; in particular, high stress concentration can be observed near the location of defects and damages and this is also prone to the localized failure and damage accumulation. For components subjected to cyclic excitations such as machine parts and bridges, pre-existing cracks or load-induced cracks under a large number of load cycles can also lead to fatigue failure at a relatively low stress level. As a result, it necessitates the comprehensive damage/fracture evaluation and failure analysis in the design procedure of those involved components to ensure their safety and integrity during the entire designed lifespan. For various classes of materials found in practices (e.g., glass, composites, concrete, rock, cast iron, etc.), the fracture-induced failure mechanism assumes in a brittle fashion and any irrecoverable deformation is merely contained in a small, localized region surrounding the cracks. An existing, well-established, mathematical model based upon the theory of linear elasticity has been found well-suited and commonly used to perform a stress analysis of bodies containing defects to provide essential information in the damage/fatigue assessments.

Conventional approaches in linear elastic fracture mechanics are based fundamentally on the dominant stress field in the vicinity of the crack front – a singular term in the Williams asymptotic expansion that involves the stress intensity factors (SIFs) and commonly termed the K-field. An obvious application of the stress intensity factors, besides the use in the prediction of crack initiation and propagation direction of crack advances, is the estimation of plastic-zone size and shape of a local region surrounding the crack front (e.g., Anderson, 2005). The plastic-zone size plays an important role in the classification of the fracture problems into either small-scale or large-scale yielding. However, there were pointed out by various investigators that the first non-singular term in the asymptotic expansion of the stress field (e.g., Williams, 1957), termed the T-stress, significantly influences both the size and shape of the plastic zone. This, therefore, necessitates the integration of the T-

stress information in the calculation of the plastic-zone size. In addition, the T-stress has also been found influencing the fracture initiation angle, the tri-axiality of the near-tip stress field, and the stability of crack propagation. Studies by Rice (1974), Du and Hancock (1991), and Sedighiani *et al.* (2011) revealed that the positive T-stress decreases the plastic-zone size and rotates its shape forward while increasing the initiation angle of crack advances and strengthening the crack-tip tri-axiality. On the contrary, presence of the negative T-stress at the crack-front renders the reverse effects. As becomes evident, the T-stress is one of essential fracture data that must be determined to accurately describe the near-tip behavior.

1.2 Background and Review

Studies towards the development of techniques for calculating the T-stress and investigation of its influence on the fracture responses and behavior using both two- and three-dimensional crack models have received significant attention from various researchers in the past several decades. Some of existing relevant investigations are briefly summarized below to shed some light on the historical background and current advances in the area, and finally indicate the existing gap of knowledge and the novel aspect of the present study.

Within the context of two-dimensional boundary value problems, Rice (1974) originally investigated the influence of the T-stress on the estimation of the plastic zone size and shape using Barrenblatt-Dugdale yielding model and conformed in this study that the T-stress significantly affects both the size and shape of the plastic zone surrounding the crack tip. Du and Hancock (1991) investigated the influence of the T-stress on the plastic zone size and shape for a plane strain crack using Von-Mises yielding criterion and they concluded that the plastic zone is enlarged and rotated forward for the negative T-stress and is reduced and rotated backward for the positive T-stress. Fett (1997) determined the T-stress in an edge cracked, rectangular, finite plate made of an isotropic, linear elastic material by first using a boundary collocation technique to construct Green's functions for a pair of normal point forces and then applied them to obtain a solution for the prescribed arbitrary normal traction. Later, Fett (1998) employed the same technique to calculate numerical results of T-stress in isotropic, linear elastic rectangular plates and circular disks containing an edged crack and a center crack subjected to both tensile and bending loads. Wang (2002) used the weight-function technique and finite element method to determine the T-stress for various test specimens including a single edge cracked plate (SECP), a double edge cracked plate (DECP) and a center cracked plate

(CCP) under uniform, linear, parabolic and cubic normal traction acting to the crack surfaces. All specimens considered in his numerical study were assumed isotropic, linear elastic. Fett and Rizzi (2006) also applied the weight-function technique and finite element method to study the T-stress of a compact tension crack (CT), a double cantilever crack (DCC), and an edge cracked bar (ECB) loaded by near-tip, arbitrarily distributed, normal traction. Fett *et al.* (2006) studied the T-stress for kinked and forked cracks in a two-dimensional isotropic plate subjected to arbitrary normal and in-plane shear traction on the crack surface by using a technique of Green's function. Zhou *et al.* (2013) employed a symplectric expansion method to determine the T-stress for an edged crack in an isotropic, linearly elastic plate bonded by two different materials. This symplectic expansion method was found to be capable of treating either mixed or complex boundary conditions. It should be remarked that while two-dimensional problems associated with cracks and bodies of various geometries and general loading conditions have been solved, the material anisotropy has not been taken into account in those previous studies.

Due to the loss of various crucial three-dimensional aspects (e.g., variation of fracture data along the crack front, full mode-mixity, stress tri-axiality ahead of the crack front, non-planarity and distortion of the crack surface, etc.) resulting from the use of two-dimensional models in the simulations, solution packages capable of fully three-dimensional stress analysis have been continuously proposed and widely employed in the fracture modeling. For T-stress calculations, several investigations have been well recognized and can be summarized below. Wang (2003) determined the T-stress for a semi-elliptical, surface-breaking crack in an isotropic, linear elastic finite thick plate subjected to tensile and bending loads at both ends. In this work, the finite element method was utilized to determine field quantities and the interaction integral formula was adopted to extract the T-stress along the crack front. In the following year, Wang and Bell (2004) extended the work of Wang (2003) to be capable of modeling more general end loading conditions such as uniform, linear, parabolic, and cubic loads. Later, Wang (2004) presented an analytical solution for the T-stress of a penny-shaped crack embedded in an isotropic linear elastic infinite body under the action of remote tension and bending loading conditions. To derive the complete elastic field, the potential-theory-based method and the Hankel integral transformation were employed. Qu and Wang (2006) investigated a corner quarter-elliptical crack in an isotropic, linear elastic thick plate under the tensile and bending loads at both ends. In their numerical study, the finite element method was utilized to perform the stress analysis whereas the interaction integral formula is

adopted to determine the T-stress along the crack front. Later, Kirilyuk and Levchuk (2007) generalized the work of Wang (2004) to obtain the elastic T-stress of a flat-elliptical crack in an isotropic, linearly elastic, infinite body under remote tension and bending by using the method of potential theory and a special collection of harmonic functions. Schütte and Molla-Abbasi (2007) and Molla-Abbasi and Schütte (2008) applied the potential-theory-based method, technique of Green's function, Hankel's transformation and a finite element method to calculate the T-stress of both penny-shaped and flat-elliptical cracks embedded in a three-dimensional isotropic infinite domain under remote mixed-mode tractions. The influence of the T-stress on estimation of the plastic zone size using the Von-Mises yielding criterion was also investigated and its significant contribution was confirmed. Lewis and Wang (2008) employed the finite element technique to compute the elastic T-stress for a circumferential crack in an isotropic finite cylinder subjected to either tensile and bending loads at its ends or uniform, linear, parabolic and cubic normal tractions on the crack surface. Recently, Meshii *et al.* (2010) also used the finite element method to determine the elastic T-stress of a semi-elliptical crack embedded in a three-dimensional isotropic finite cylinder under uniform, linear, parabolic and cubic normal tractions on the crack surface.

On the basis of an extensive literature survey, most of existing studies were restricted mainly to cracked bodies made of isotropic, linear elastic materials. Use of this idealized constitutive model in the fracture analysis can significantly simplify the solution methodology and computational effort but, at the same time, limits the capability to treat various modern construction materials such as smart materials and composites whose properties and behavior are generally anisotropic in nature. The influence of material anisotropy on both the values and distribution along the crack front has not been well-recognized and still requires further investigations. This existing gap of knowledge encourages the present investigation.

1.3 Research Objectives

The key objectives of the proposed research are (i) to construct an analytical solution of the T-stress for cracks in anisotropic elastic media and (ii) to investigate the influence of material properties and loading conditions on both values and distribution of the T-stress along the crack front.

1.4 Research Scope

The proposed investigation is conducted within the following contexts: (i) the body is infinite, three-dimensional, free of body force and remote loading, and made of homogeneous, transversely isotropic, linearly elastic materials with fully prescribed material constants; (ii) the crack is penny-shaped and oriented perpendicular to the axis of material symmetry; and (iii) the crack is subjected only to self-equilibrated normal and shear traction.

1.5 Research Methodology

Methodology, procedures, and fundamental theories involved in this research can be briefly summarized as follows:

1.5.1 basic field equations governing all field quantities follow a theory of linear elasticity;

1.5.2 two special boundary value problems associated with a penny-shaped crack subjected to a pair of concentrated normal forces and a pair of concentrated tangential forces are formulated using selected basic field equations;

1.5.3 the same potential-theory-based technique as employed by Fabrikant (1989) is adopted to obtain closed-form solutions for the stress field of two fundamental boundary value problems;

1.5.4 appropriate derivative and limit process is applied along with the obtained stress field to derive the T-stress Green's function;

1.5.5 a method of superposition is utilized to form a general integral expression for calculating the T-stress of a penny-shaped crack subjected to arbitrary applied traction;

1.5.6 a selected numerical quadrature is adopted to efficiently and accurately evaluate involved strongly singular integrals; and

1.5.7 the influence of material properties and loading conditions on the values and distribution of the T-stress along the crack front is fully investigated.

1.6 Research Significance

The significant contribution of the proposed research is to provide an analytical solution of T-stress for a penny-shaped crack in transversely isotropic linearly elastic

infinite medium under arbitrary prescribed point-wise self-equilibrate normal and shear tractions. These results can be used not only to perform parametric study to understand the influence of material properties and loading conditions on values and distribution of the T-stress along the crack front but also to generate benchmark or reference solutions for comparison purposes in the development of numerical techniques for determining the T-stress for general cases.

CHAPTER II

THEORETICAL CONSIDERATIONS

This chapter summarizes the clear description of the boundary value problems considered in the present investigation, basic governing field equations, and a closed form solution of the stress field for fundamental problems essential for the development of the T-stress Green's function.

2.1 Problem Description

Consider a penny-shaped crack of a radius a embedded in a three-dimensional infinite medium as shown schematically in Figure 2.1. The body is made of a homogeneous, transversely isotropic, linear elastic material with the elastic moduli fully prescribed. The axis of material symmetry is assumed perpendicular to the crack surface. The body is free of the body force and remote loading whereas the crack is subjected to arbitrarily distributed, self-equilibrated traction $\boldsymbol{t}^0$ (i.e., the sum of the traction on the crack surface identically vanishes).

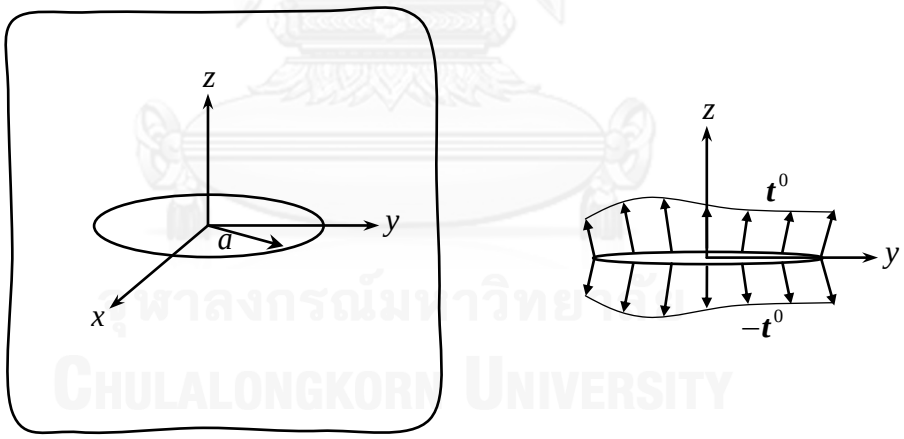

Figure 2.1: Schematic of penny-shaped crack of radius a embedded in a transversely isotropic medium and subjected to arbitrarily distributed traction

For convenience in the development presented further below, a reference Cartesian coordinate system $\{\mathbf{0}; x, y, z\}$ and the corresponding cylindrical coordinate system $\{\mathbf{0}; \rho, \phi, z\}$ are chosen such that the origin $\mathbf{0}$ is located at the center of the penny-shaped crack, the z-axis directs normal to the crack surface, and x- and y-axes follow the right hand rule.

2.2 Basic Field Equations

The fundamental theory of linear elasticity is utilized to formulate the basic equations governing all involved field quantities. Equilibrium equations, in the absence of the body force, can be given explicitly in terms of components of the stress tensor $\boldsymbol{\sigma}$ in the reference Cartesian coordinate system as

$$\frac{\partial \sigma_{xx}}{\partial x}+\frac{\partial \sigma_{xy}}{\partial y}+\frac{\partial \sigma_{xz}}{\partial z}=0 \tag{2.1a}$$

$$\frac{\partial \sigma_{xy}}{\partial x}+\frac{\partial \sigma_{yy}}{\partial y}+\frac{\partial \sigma_{yz}}{\partial z}=0 \tag{2.1b}$$

$$\frac{\partial \sigma_{xz}}{\partial x}+\frac{\partial \sigma_{yz}}{\partial y}+\frac{\partial \sigma_{zz}}{\partial z}=0 \tag{2.1c}$$

The strain tensor $\boldsymbol{\varepsilon}$ and the displacement vector $\boldsymbol{u}$ are related by the following infinitesimal (or linearized) kinematics:

$$\varepsilon_{xx}=\frac{\partial u_x}{\partial x} \tag{2.2a}$$

$$\varepsilon_{yy}=\frac{\partial u_y}{\partial y} \tag{2.2b}$$

$$\varepsilon_{zz}=\frac{\partial u_z}{\partial z} \tag{2.2c}$$

$$\varepsilon_{xy}=\frac{1}{2}\left(\frac{\partial u_x}{\partial y}+\frac{\partial u_y}{\partial x}\right) \tag{2.2d}$$

$$\varepsilon_{yz}=\frac{1}{2}\left(\frac{\partial u_y}{\partial z}+\frac{\partial u_z}{\partial y}\right) \tag{2.2e}$$

$$\varepsilon_{xz}=\frac{1}{2}\left(\frac{\partial u_x}{\partial z}+\frac{\partial u_z}{\partial x}\right) \tag{2.2f}$$

For a transversely isotropic linear elastic material, the relationship between the stress and strain are given by

$$\sigma_{xx}=A_{11}\varepsilon_{xx}+\left(A_{11}-2A_{66}\right)\varepsilon_{yy}+A_{13}\varepsilon_{zz} \tag{2.3a}$$

$$\sigma_{yy}=\left(A_{11}-2A_{66}\right)\varepsilon_{xx}+A_{11}\varepsilon_{yy}+A_{13}\varepsilon_{zz} \tag{2.3b}$$

$$\sigma_{zz}=A_{13}\varepsilon_{xx}+A_{13}\varepsilon_{yy}+A_{33}\varepsilon_{zz} \tag{2.3c}$$

$$\sigma_{xy} = 2A_{66}\varepsilon_{xy} \tag{2.3d}$$

$$\sigma_{yz} = 2A_{44}\varepsilon_{yz} \tag{2.3e}$$

$$\sigma_{xz} = 2A_{44}\varepsilon_{xz} \tag{2.3f}$$

where A_{11}, A_{13}, A_{33}, A_{44} and A_{66} are known non-zero elastic constants. By combining field equations (2.1)–(2.3), it leads to three equilibrium equations in terms of the displacement (i.e., Navier's equations)

$$A_{11}\frac{\partial^2 u_x}{\partial x^2} + A_{66}\frac{\partial^2 u_x}{\partial y^2} A_{44}\frac{\partial^2 u_x}{\partial z^2} + \left(A_{11} - A_{66}\right)\frac{\partial^2 u_y}{\partial x \partial y} + \left(A_{13} + A_{44}\right)\frac{\partial^2 u_z}{\partial x \partial z} = 0 \tag{2.4a}$$

$$A_{66}\frac{\partial^2 u_y}{\partial x^2} + A_{11}\frac{\partial^2 u_y}{\partial y^2} A_{44}\frac{\partial^2 u_y}{\partial z^2} + \left(A_{11} - A_{66}\right)\frac{\partial^2 u_x}{\partial x \partial y} + \left(A_{13} + A_{44}\right)\frac{\partial^2 u_z}{\partial y \partial z} = 0 \tag{2.4b}$$

$$A_{44}\left[\frac{\partial^2 u_z}{\partial x^2} + \frac{\partial^2 u_z}{\partial y^2}\right] + A_{33}\frac{\partial^2 u_z}{\partial z^2} + \left(A_{13} + A_{44}\right)\left[\frac{\partial^2 u_x}{\partial x \partial z} + \frac{\partial^2 u_y}{\partial y \partial z}\right] = 0 \tag{2.4c}$$

A system of partial differential equations (2.4) along with the prescribed information of the applied traction on the crack surfaces $\boldsymbol{t}^0$ forms a complete boundary value problem associated with that described in section 2.1.

2.3 Stress Field of Two Fundamental Problems

Instead of directly determining the complete elastic field and the corresponding T-stress along the crack front of the penny-shaped crack under arbitrarily distributed applied traction, it is appealing to invoke the linearity of the problem and also employ the method of superposition. Following this strategy, two fundamental problems associated with the penny-shaped crack subjected to a pair of self-equilibrated, unit concentrated forces normal and tangent to the crack surfaces must be solved analytically. The T-stresses for these two special cases, termed the T-stress Green's function, are then extracted in a closed form from the known stress field. The final expression of the T-stresses for the original problem with the general applied traction can subsequently be established in terms of a single surface integral (see details in Chapter III).

2.3.1 A pair of self-equilibrated unit point forces normal to crack surface

Consider a penny-shaped crack subjected to a pair of self-equilibrated unit normal point forces at a point on the upper crack surface, denoted by cylindrical

coordinates $(\rho_0, \phi_0, 0^+)$, and a point on the lower crack surface, denoted by cylindrical coordinates $(\rho_0, \phi_0, 0^-)$, as shown in Figure 2.2.

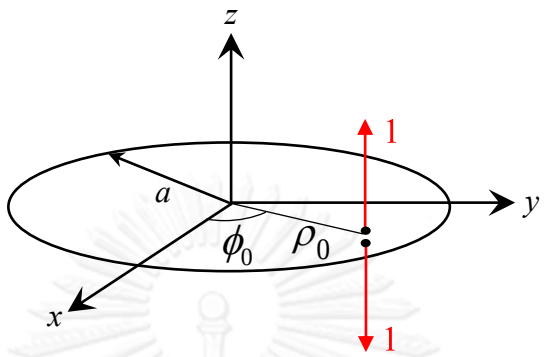

Figure 2.2: Penny-shaped crack subjected to a pair of self-equilibrated unit concentrated forces normal to the crack surface

To determine the complete elastic field of this fundamental boundary value problem, several analytical techniques can be employed. A special potential-theory-based technique proposed by Fabrikant (1989) has been found efficient and can yield the closed form solution of this particular problem involving only elementary functions. The final explicit solution for the stress at any point $(\rho, \phi, z), z \geq 0$ derived by Fabrikant (1989) is given by

$$\sigma_1^n(r,\theta,z) = \frac{2}{\pi^2(\gamma_1-\gamma_2)}\left\{\left(\frac{\gamma_1}{(m_1+1)\gamma_3^2}-\frac{1}{\gamma_1}\right)f_3(z_1) - \left(\frac{\gamma_2}{(m_2+1)\gamma_3^2}-\frac{1}{\gamma_2}\right)f_3(z_2)\right\} \tag{2.5a}$$

$$\sigma_2^n(r,\theta,z) = \frac{4}{\pi}HA_{66}\left(\frac{\gamma_1}{(m_1-1)}f_4(z_1)+\frac{\gamma_2}{(m_2-1)}f_4(z_2)\right) \tag{2.5b}$$

$$\sigma_z^n(r,\theta,z) = \frac{1}{\pi^2(\gamma_1-\gamma_2)}\left(\gamma_1 f_3(z_1)-\gamma_2 f_3(z_2)\right) \tag{2.5c}$$

$$\tau_z^n(r,\theta,z) = \frac{1}{\pi^2(\gamma_1-\gamma_2)}\left(f_5(z_1)-f_5(z_2)\right) \tag{2.5d}$$

where $z_i = z/\gamma_i$ for $i = 1, 2$; the superscript "n" is used to emphasize that the given functions are associated with a pair of unit *normal* concentrate forces; material-dependent parameters are defined by

$$\gamma_3^2 = \sqrt{A_{44}/A_{66}} \tag{2.6a}$$

$$H = \frac{(\gamma_1+\gamma_2)A_{11}}{2\pi(A_{11}A_{33}-A_{13}^2)} \tag{2.6b}$$

$$A_{11}\gamma_k^2 = A_{44} + m_k(A_{13}+A_{44}) \text{ for } k=1,2 \tag{2.6c}$$

$$m_1 m_2 = 1; \tag{2.6d}$$

and σ_1^n, σ_2^n and τ_z^n are given by

$$\sigma_1^n = \sigma_{xx}^n + \sigma_{yy}^n = \sigma_{\rho\rho}^n + \sigma_{\phi\phi}^n \tag{2.7a}$$

$$\sigma_2^n = \sigma_{xx}^n - \sigma_{yy}^n + 2i\sigma_{xy} = (\sigma_{\rho\rho}^n - \sigma_{\phi\phi}^n + 2i\sigma_{\rho\phi}^n)e^{2i\phi} \tag{2.7b}$$

$$\tau_z^n = \sigma_{xz}^n + i\sigma_{yz}^n \tag{2.7c}$$

Explicit expressions of functions f_3, f_4 and f_5 appearing in (2.5) in terms of elementary functions are given by

$$f_3(z) = \left\{ -\frac{z}{R_0^3}\tan^{-1}\left(\frac{h}{R_0}\right) + \frac{h}{z\left(R_0^2+h^2\right)}\left[\frac{\rho^2-l_1^2}{l_2^2-l_1^2} - \frac{z^2}{R_0^2}\right]\right\} \tag{2.8a}$$

$$\begin{aligned} f_4(z) = {} & \frac{\left(a^2-\rho_0^2\right)^{1/2}}{\bar{q}\,\bar{s}}\left(\frac{\rho_0 e^{i\phi_0}}{\bar{s}^2} - \frac{2}{\bar{q}}\right)\tan^{-1}\left(\frac{\bar{s}}{\left(l_2^2-a^2\right)^{1/2}}\right) \\ & + \frac{z\left(3R_0^2-z^2\right)}{\bar{q}^2 R_0^3}\tan^{-1}\left(\frac{h}{R_0}\right) - \frac{\left(a^2-\rho_0^2\right)^{1/2}\left(l_2^2-a^2\right)^{1/2}\rho_0 e^{i\phi_0}}{\bar{q}\,\bar{s}^2\left[l_2^2-\rho\rho_0 e^{-i(\phi-\phi_0)}\right]} \\ & + \frac{zh}{R_0^2+h^2}\left[\frac{q}{\bar{q}R_0^2} - \frac{\rho^2 e^{2i\phi}}{\left(l_2^2-l_1^2\right)\left(l_2^2-\rho^2\right)}\right] \end{aligned} \tag{2.8b}$$

$$f_5(z) = -\left\{\frac{\rho e^{i\phi}-\rho_0 e^{i\phi_0}}{R_0^3}\tan^{-1}\left(\frac{h}{R_0}\right) + \frac{h}{R_0^2+h^2}\left[\frac{\rho e^{i\phi}}{l_2^2-l_1^2} + \frac{\rho e^{i\phi}-\rho_0 e^{i\phi_0}}{R_0^2}\right]\right\} \tag{2.8c}$$

where $\bar{f}$ denotes the complex conjugate of f and

$$l_1 = \frac{1}{2}\left\{\sqrt{(\rho+a)^2+z^2} - \sqrt{(\rho-a)^2+z^2}\right\} \tag{2.9a}$$

$$l_2 = \frac{1}{2}\left\{\sqrt{(\rho+a)^2+z^2} + \sqrt{(\rho-a)^2+z^2}\right\} \tag{2.9b}$$

$$h = \frac{\sqrt{a^2 - l_1^2}\sqrt{a^2 - \rho_0^2}}{a} \tag{2.9c}$$

$$q = \rho e^{i\phi} - \rho_0 e^{i\phi_0} \tag{2.9d}$$

$$\overline{q} = \rho e^{-i\phi} - \rho_0 e^{-i\phi_0} \tag{2.9e}$$

$$\overline{s} = \sqrt{a^2 - \rho\rho_0 e^{-i(\phi-\phi_0)}} \tag{2.9f}$$

$$R_0 = \sqrt{\rho^2 + \rho_0^2 - 2\rho\rho_0\cos(\phi - \phi_0) + z^2} \tag{2.9g}$$

2.3.2 A pair of self-equilibrated unit point forces tangent to crack surface

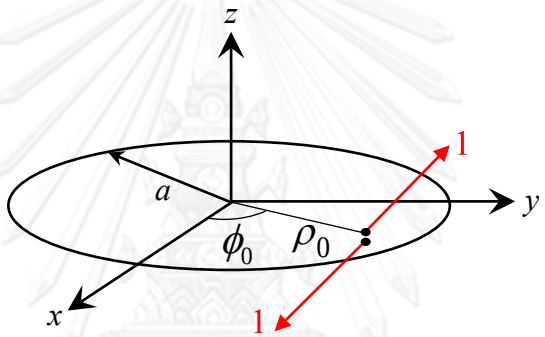

Figure 2.3: Penny-shaped crack subjected to a pair of self-equilibrated unit point forces tangential to the crack surface

Consider, next, a penny-shaped crack subjected to a pair of self-equilibrated unit tangential point forces at a point on the upper crack surface, denoted by cylindrical coordinates $(\rho_0, \phi_0, 0^+)$, and a point on the lower crack-surface, denoted by cylindrical coordinates $(\rho_0, \phi_0, 0^-)$, as shown in Figure 2.3. Components of the unit point force in the x- and y-directions are denoted by T_x and T_y, respectively. Similar to the previous case, the complete elastic field within the medium for this particular case can be obtained by applying the potential-theory-based technique to solve the governing equations (2.4) analytically. The explicit results for the stress field obtained by Fabrikant (1989) are given, here, by

$$\sigma_1^t(r,\theta,z) = \mathrm{Re}\left\{\frac{2\gamma_1\gamma_2}{\pi^2(\gamma_1-\gamma_2)}\sum_{k=1}^{2}(-1)^{k+1}\left[\frac{1}{\gamma_3^2(m_k+1)} - \frac{1}{\gamma_k^2}\right] \times\left[\bar{f}_5(z_k) + \frac{G_2}{G_1}\bar{f}_{10}(z_k)\right]T\right\} \tag{2.10a}$$

$$\sigma_2^t(r,\theta,z) = -\frac{2}{\pi} A_{66} H \gamma_1 \gamma_2 \sum_{k=1}^{2} \frac{1}{(m_k - 1)} \left\{ \left(f_5(z_k) + \frac{G_2}{G_1} \overline{f}_{13}(z_k) \right) T \right.$$
$$\left. + \left(f_{11}(z_k) + \frac{G_2}{G_1} f_{12}(z_k) \right) \overline{T} \right\} - \frac{1}{\pi^2 \gamma_3} \left\{ \left(-f_5(z_3) + \frac{G_2}{G_1} \overline{f}_{13}(z_3) \right) T \right. \qquad (2.10b)$$
$$\left. + \left(f_{11}(z_3) - \frac{G_2}{G_1} f_{12}(z_3) \right) \overline{T} \right\}$$

$$\sigma_z^t(r,\theta,z) = \mathrm{Re}\left\{ \frac{\gamma_1 \gamma_2}{\pi^2 (\gamma_1 - \gamma_2)} \sum_{k=1}^{2} (-1)^{k+1} \left(\overline{f}_5(z_k) + \frac{G_2}{G_1} \overline{f}_{10}(z_k) \right) T \right\} \qquad (2.10c)$$

$$\tau_z^t(r,\theta,z) = \frac{\gamma_1 \gamma_2}{2\pi^2 (\gamma_1 - \gamma_2)} \sum_{k=1}^{2} \frac{(-1)^k}{\gamma_k} \left\{ \left(f_3(z_k) + \frac{G_2}{G_1} \overline{f}_{14}(z_k) \right) T \right.$$
$$\left. + \left(-f_4(z_k) + \frac{G_2}{G_1} f_{15}(z_k) \right) \overline{T} \right\} - \frac{1}{\pi^2} \left\{ \left(-f_3(z_3) - \frac{G_2}{G_1} \overline{f}_{14}(z_3) \right) T \right. \qquad (2.10d)$$
$$\left. + \left(f_4(z_3) + \frac{G_2}{G_1} f_{15}(z_3) \right) \overline{T} \right\}$$

where the superscript "t" is used to emphasize that the quantities are associated with a pair of unit *tangential* concentrated forces; $\mathrm{Re}\{f\}$ denotes the real part of the function f; $T = T_x + iT_y$, $\overline{T} = T_x - iT_y$, $G_1 = \beta + \gamma_1\gamma_2 H$, $G_2 = \beta - \gamma_1\gamma_2 H$, $\beta = \gamma_3 / 2\pi A_{44}$; and the functions f_{10}, f_{11}, f_{12}, f_{13}, f_{14}, and f_{15} are defined by

$$f_{10}(z) = -\frac{h\rho e^{i\phi}(3l_2^2 - a^2 t)}{(l_2^2 - l_1^2)(l_2^2 - a^2 t)^2} \qquad (2.11a)$$

$$f_{11}(z) = \frac{1}{\overline{q}} \left\{ \frac{3R_0^4 + 6R_0^2 z^2 - z^4}{R_0^3 \overline{q}^2} \tan^{-1}\left(\frac{h}{R_0}\right) - \left(a^2 - \rho_0^2\right)^{1/2} \left[\frac{z}{\overline{s}} \left(\frac{8}{\overline{q}^2} \right.\right.\right.$$
$$\left. - \frac{4\rho_0 e^{i\phi_0}}{\overline{s}^2 \overline{q}} + \frac{3\rho_0^2 e^{2i\phi_0}}{\overline{s}^4} \right) \tan^{-1}\left(\frac{\overline{s}}{\sqrt{l_2^2 - a^2}} \right) - \frac{e^{i\phi}}{\rho} \left(\frac{2e^{i\phi}}{\rho} + \frac{3}{\overline{q}} \right)$$
$$\left. - \frac{3\left(\overline{\xi} - 1\right)^{1/2}}{\overline{q}^2} \left(\tan^{-1} \frac{1}{\sqrt{\overline{\xi} - 1}} - \tan^{-1} \frac{\sqrt{a^2 - l_1^2}}{a\sqrt{\overline{\xi} - 1}} \right) \right] \qquad (2.11b)$$
$$+ \frac{ha^2 e^{i\phi}}{\rho \overline{s}^2} \left[\frac{2\rho_0 e^{i\phi_0}}{\overline{s}^2} - \frac{2e^{i\phi}}{\rho} - \frac{2}{\overline{q}} + \left(\frac{\rho_0 e^{i\phi_0}}{\overline{s}^2} - \frac{2}{\overline{q}} \right) \frac{\left(l_2^2 - a^2\right)\overline{t}}{l_2^2 - a^2 \overline{t}} \right]$$
$$\left. - \frac{h}{R_0^2 + h^2} \left[\frac{\overline{q}\rho e^{3i\phi}}{l_2^2 - l_1^2} + \frac{e^{i\phi}\left(l_2^2 - \rho^2\right)}{\rho \overline{q}} - \frac{z^2 q}{R_0^2 \overline{q}} + 2e^{2i\phi} \right] \right\}$$

$$f_{12}(z)=\frac{1}{\overline{q}}\left(a^2-\rho_0^2\right)^{1/2}\left\{\frac{3\left(\overline{\xi}-1\right)^{1/2}}{\overline{q}^2}\left[\tan^{-1}\left(\frac{1}{\left(\overline{\xi}-1\right)^{1/2}}\right)-\tan^{-1}\left(\frac{\left(a^2-l_1^2\right)^{1/2}}{a\left(\overline{\xi}-1\right)^{1/2}}\right)\right]\right.$$
$$-\frac{e^{2i\phi}\left(a^2-l_1^2\right)^{1/2}}{a\left(l_2^2-l_1^2\right)}\left[\frac{l_2^2+\rho^2}{l_2^2-\rho\rho_0e^{i(\phi-\phi_0)}}+\frac{2\rho^2\left(l_2^2-a^2\right)}{\left(l_2^2-\rho\rho_0e^{i(\phi-\phi_0)}\right)^2}+1\right] \tag{2.11c}$$
$$\left.+\frac{e^{i\phi}}{\rho}\left[\frac{3}{\overline{q}}+\frac{2e^{i\phi}}{\rho}-\frac{\left(a^2-l_1^2\right)^{1/2}}{a}\left(\frac{l_2^2+2\rho^2}{\overline{q}\left(l_2^2-\rho\rho_0e^{i(\phi-\phi_0)}\right)}+2\left(\frac{1}{\overline{q}}+\frac{e^{i\phi}}{\rho}\right)\right)\right]\right\}$$

$$\overline{f}_{13}(z)=-h\left\{\frac{a^2}{\overline{s}^2}\rho_0e^{i\phi_0}\left[\frac{15\left(l_2^2-a^2\right)^{1/2}}{\overline{s}^5}\tan^{-1}\left(\frac{\overline{s}}{\left(l_2^2-a^2\right)^{1/2}}\right)-\frac{15}{\overline{s}^4}\right.\right. \tag{2.11d}$$
$$\left.\left.+\frac{5}{\overline{s}^2\left(l_2^2-a^2\overline{t}\right)}+\frac{2\overline{t}}{\left(l_2^2-a^2\overline{t}\right)^2}\right]+\frac{\rho e^{i\phi}\left(3l_2^2-a^2\overline{t}\right)}{\left(l_2^2-l_1^2\right)\left(l_2^2-a^2\overline{t}\right)^2}\right\}$$

$$f_{14}(z)=\frac{\left(a^2-\rho_0^2\right)^{1/2}}{a^3\left(1-t\right)}\left\{\frac{a\left(l_2^2-a^2\right)^{1/2}}{\left(l_2^2-l_1^2\right)\left(l_2^2-\rho\rho_0e^{i(\phi-\phi_0)}\right)}\left[\frac{3\left(l_2^2-l_1^2t\right)}{1-t}\right.\right.$$
$$\left.\left.+\frac{\rho\rho_0e^{i(\phi-\phi_0)}\left(2l_2^2+l_1^2t-3\rho^2\right)}{l_2^2-\rho\rho_0e^{i(\phi-\phi_0)}}\right]-\frac{3}{\left(1-t\right)^{3/2}}\tan^{-1}\left(\frac{a\left(1-t\right)^{1/2}}{\left(l_2^2-a^2\right)^{1/2}}\right)\right\} \tag{2.11e}$$

$$f_{15}(z)=\frac{\rho^2e^{2i\phi}\left(a^2-\rho_0^2\right)^{1/2}\left(l_2^2-a^2\right)^{1/2}\left(3l_2^2-\rho\rho_0e^{i(\phi-\phi_0)}\right)}{l_2^2\left(l_2^2-l_1^2\right)\left(l_2^2-\rho\rho_0e^{i(\phi-\phi_0)}\right)^2} \tag{2.11f}$$

with $t=\rho\rho_0e^{i(\phi-\phi_0)}/a^2$ and $\xi=\rho e^{i(\phi-\phi_0)}/\rho_0$.

CHAPTER III

DETERMINATION OF T-STRESS

In this chapter, the asymptotic expansion of the stress field in the vicinity of the crack front, the derivation of the T-stress Green's function for two fundamental problems indicated in Chapter II, the integral formula of the T-stress for a penny-shaped crack under self-equilibrated, arbitrarily distributed traction, and the numerical treatment of involved strongly singular integrals are presented.

3.1 Asymptotic Expansion of Near-tip Field

By performing the near-tip asymptotic analysis similar to the original work of Williams (1957), the stress field in the vicinity of a point $\boldsymbol{x}_c$ on the crack front admits the following representation (with respect to the local reference coordinate system $\{\boldsymbol{x}_c; x_1, x_2, x_3\}$ with the origin at $\boldsymbol{x}_c$ and orthonormal base vectors $\{\boldsymbol{e}_1, \boldsymbol{e}_2, \boldsymbol{e}_3\}$ being defined such that the $x_1 - x_2$ plane is normal to the crack front at point $\boldsymbol{x}_c$ and the $x_1 - x_3$ plane is tangent to the crack surface at point $\boldsymbol{x}_c$; also see Figure 3.1):

$$\sigma_{ij}(\boldsymbol{x}_c; r, \theta) = \frac{1}{\sqrt{r}} \sigma_{ij}^{K}(\boldsymbol{x}_c; \theta) + \sigma_{ij}^{T}(\boldsymbol{x}_c; \theta) + \sum_{m=1}^{\infty} r^{m/2} \sigma_{ij}^{m}(\boldsymbol{x}_c; \theta) \tag{3.1}$$

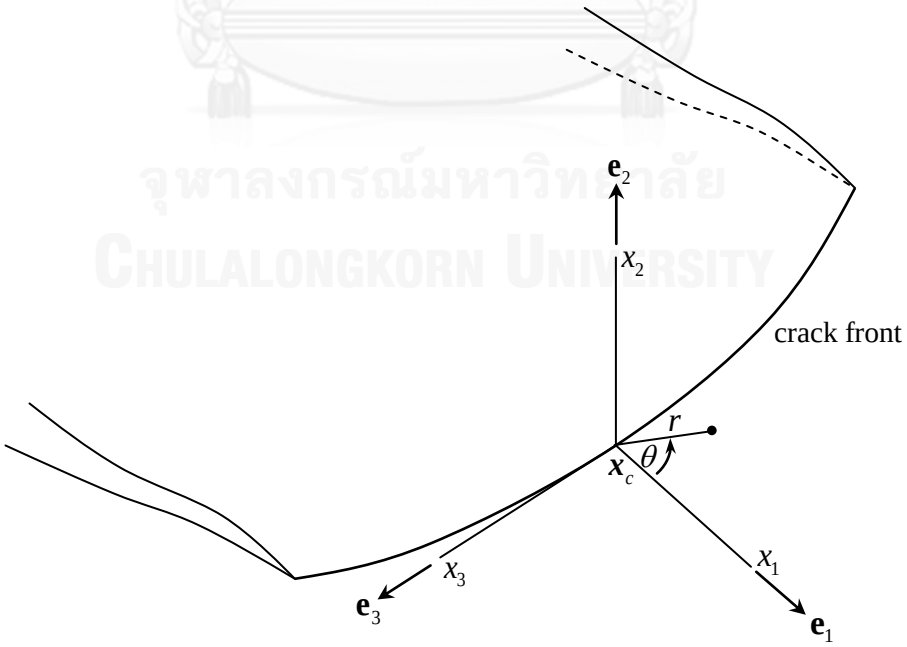

Figure 3.1: Schematic of crack front and local coordinate system $\{\boldsymbol{x}_c; x_1, x_2, x_3\}$

where (r,θ) denotes standard polar coordinates of a point on the $x_1 - x_2$ plane; $\sigma_{ij}(\boldsymbol{x}_c; r,\theta)$ denotes the stress at the point (r,θ) referring to the local coordinate system $\{\boldsymbol{x}_c; x_1, x_2, x_3\}$; and σ_{ij}^K, σ_{ij}^T and σ_{ij}^m are functions independent of the radial distance from the crack front r. It should be apparent from the expansion (3.1) that the first term indicates that the stress predicted by linear elasticity theory is singular at the crack front of order $1/\sqrt{r}$; the second term is independent of the coordinate r; and the remaining higher order terms vanish at the crack front. It is worth noting that while the angular variation of the functions σ_{ij}^K, σ_{ij}^T and σ_{ij}^m can be obtained from the asymptotic analysis, their dependence on material properties, geometries of cracks and bodies, and boundary and loading conditions still requires the full analysis of the associated boundary value problem. Once the complete stress field is determined, the unknown information of the functions σ_{ij}^K, σ_{ij}^T and σ_{ij}^m can readily be obtained via a standard series expansion procedure.

3.2 Definition of T-stress

Let $T_{ij}(\boldsymbol{x}_c)$ be a symmetric, second order tensor defined, with respect to the local coordinate system $\{\boldsymbol{x}_c; x_1, x_2, x_3\}$, by

$$T_{ij}(\boldsymbol{x}_c) = \sigma_{ij}^T(\boldsymbol{x}_c; \theta = 0) \tag{3.2}$$

It is evident from (3.1) that the tensor $T_{ij}(\boldsymbol{x}_c)$ represents the finite part of the stress $\sigma_{ij}(\boldsymbol{x}_c; r = 0, \theta = 0)$ at the point $\boldsymbol{x}_c$ on the crack front. Due to the continuity condition of the finite part of the stress $\sigma_{ij}(\boldsymbol{x}_c; r,\theta)$ at point along the crack front, it can be verified that the components $T_{12}(\boldsymbol{x}_c)$, $T_{22}(\boldsymbol{x}_c)$ and $T_{23}(\boldsymbol{x}_c)$ are known a priori and equal to the prescribed traction on the crack surface at the point $\boldsymbol{x}_c$. The remaining components, $T_{11}(\boldsymbol{x}_c)$, $T_{33}(\boldsymbol{x}_c)$ and $T_{13}(\boldsymbol{x}_c)$, are unknown a priori and defined as the T-stress components. Once the T-stress components, $T_{11}(\boldsymbol{x}_c)$, $T_{33}(\boldsymbol{x}_c)$ and $T_{13}(\boldsymbol{x}_c)$, are solved, the first non-singular term $\sigma_{ij}^T(\boldsymbol{x}_c;\theta)$ in the representation (3.1) is completely known.

From the definition (3.2) and the expansion (3.1), the T-stress components $T_{11}(\boldsymbol{x}_c)$, $T_{33}(\boldsymbol{x}_c)$ and $T_{13}(\boldsymbol{x}_c)$ can be obtained from the stress field $\sigma_{ij}(\boldsymbol{x}_c; r,\theta)$ in the vicinity of the crack front through the following relations:

$$T_{11}(\boldsymbol{x}_c) = 2\lim_{r\to 0}\sqrt{r}\frac{\partial}{\partial r}\sqrt{r}\sigma_{11}(\boldsymbol{x}_c; r, \theta = 0) \tag{3.3}$$

$$T_{33}(\boldsymbol{x}_c) = 2\lim_{r\to 0}\sqrt{r}\,\frac{\partial}{\partial r}\sqrt{r}\sigma_{33}(\boldsymbol{x}_c; r, \theta = 0) \tag{3.4}$$

$$T_{13}(\boldsymbol{x}_c) = 2\lim_{r\to 0}\sqrt{r}\,\frac{\partial}{\partial r}\sqrt{r}\sigma_{13}(\boldsymbol{x}_c; r, \theta = 0) \tag{3.5}$$

The formula (3.3)-(3.5) allow the T-stress to be computed from the known or solved stress field of a cracked body.

3.3 T-stress Green's function for a pair of unit normal point forces

Since the complete stress field for an infinite medium containing a penny-shaped crack subjected to a pair of self-equilibrated, normal concentrated forces is available as indicated in section 2.3.1, the T-stress Green's function can then be obtained using the formula (3.3)-(3.5). In the derivation, following intermediate results have been derived and employed:

$$\lim_{z\to 0}\frac{\sqrt{a-l_1}}{z} = \sqrt{\frac{a}{2}}\,\frac{1}{\sqrt{\rho^2-a^2}} \tag{3.6}$$

$$\lim_{z\to 0}\frac{zh}{l_2-\rho} = \frac{2\sqrt{\rho^2-a^2}\sqrt{a^2-\rho_0^2}}{\rho} \tag{3.7}$$

The functions f_3, f_4 and f_5 evaluated at $z=0$ are then given by

$$f_3(z=0) = \frac{\sqrt{a^2-\rho_0^2}}{\sqrt{\rho^2-a^2}\left(R_0^0\right)^2} \tag{3.8}$$

$$\begin{aligned} f_4(z=0) = {} & \frac{\sqrt{a^2-\rho_0^2}}{\overline{q}\;\overline{s}}\left(\frac{\rho_0 e^{i\phi_0}}{\overline{s}^2}-\frac{2}{\overline{q}}\right)\tan^{-1}\left(\frac{\overline{s}}{\sqrt{\rho^2-a^2}}\right) \\ & -\frac{\sqrt{\rho^2-a^2}\sqrt{a^2-\rho_0^2}\,\rho_0 e^{i\phi_0}}{\overline{q}\;\overline{s}^2\left(\rho^2-\rho\rho_0 e^{-i(\phi-\phi_0)}\right)}-\frac{e^{2i\phi}\sqrt{a^2-\rho_0^2}}{\left(R_0^0\right)^2\sqrt{\rho^2-a^2}} \end{aligned} \tag{3.9}$$

$$f_5(z=0) = 0 \tag{3.10}$$

where the function R_0^0 is defined by

$$R_0^0 = R_0(z=0) = \sqrt{\rho^2+\rho_0^2-2\rho\rho_0\cos(\phi-\phi_0)} \tag{3.11}$$

By applying the results (3.8)-(3.10) to (2.5), it yields the stress at any point along the plane $z=0$

$$\sigma_1^n(z=0)=\Phi\frac{\sqrt{a^2-\rho_0^2}}{\sqrt{\rho^2-a^2}\left(R_0^0\right)^2} \tag{3.12}$$

$$\begin{aligned}\sigma_2^n(z=0)=\Gamma\Bigg\{&\frac{\sqrt{a^2-\rho_0^2}}{\bar{q}\,\bar{s}}\left(\frac{\rho_0 e^{i\phi_0}}{\bar{s}^2}-\frac{2}{\bar{q}}\right)\tan^{-1}\left(\frac{\bar{s}}{\sqrt{\rho^2-a^2}}\right)\\&-\frac{\sqrt{\rho^2-a^2}\sqrt{a^2-\rho_0^2}\rho_0 e^{i\phi_0}}{\bar{q}\,\bar{s}^2\left(\rho^2-\rho\rho_0 e^{-i(\phi-\phi_0)}\right)}-\frac{e^{2i\phi}\sqrt{a^2-\rho_0^2}}{\left(R_0^0\right)^2\sqrt{\rho^2-a^2}}\Bigg\}\end{aligned} \tag{3.13}$$

$$\sigma_z^n(z=0)=\frac{1}{\pi^2}\frac{\sqrt{a^2-\rho_0^2}}{\sqrt{\rho^2-a^2}\left(R_0^0\right)^2} \tag{3.14}$$

$$\tau_z^n(z=0)=0 \tag{3.15}$$

where Φ and Γ are material-dependent parameters defined by

$$\Phi=\frac{2}{\pi^2(\gamma_1-\gamma_2)}\left\{\left(\frac{\gamma_1}{(m_1+1)\gamma_3^2}-\frac{\gamma_2}{(m_2+1)\gamma_3^2}\right)-\left(\frac{1}{\gamma_1}-\frac{1}{\gamma_2}\right)\right\} \tag{3.16}$$

$$\Gamma=\frac{4HA_{66}}{\pi}\left\{\frac{\gamma_1}{m_1-1}+\frac{\gamma_2}{m_2-1}\right\} \tag{3.17}$$

By defining $\hat{r}=\rho-a$, it can readily be verified for $\rho_0\neq a$ that

$$\lim_{r\to 0}\sqrt{r}\frac{\partial}{\partial r}\sqrt{r}\left\{\frac{\sqrt{a^2-\rho_0^2}}{\sqrt{\rho^2-a^2}}\right\}=0 \tag{3.18}$$

$$\lim_{r\to 0}\sqrt{r}\frac{\partial}{\partial r}\sqrt{r}\left\{\frac{\sqrt{\rho^2-a^2}\sqrt{a^2-\rho_0^2}}{\bar{q}\,\bar{s}^2\left(\rho^2-\rho\rho_0 e^{-i(\phi-\phi_0)}\right)}\right\}=0 \tag{3.19}$$

$$\begin{aligned}\lim_{r\to 0}\sqrt{r}\frac{\partial}{\partial r}\sqrt{r}&\left\{\frac{\sqrt{a^2-\rho_0^2}}{\bar{q}\,\bar{s}}\left(\frac{\rho_0 e^{i\phi_0}}{\bar{s}^2}-\frac{2}{\bar{q}}\right)\tan^{-1}\left(\frac{\bar{s}}{\sqrt{r(r+2a)}}\right)\right\}\\&=\pi\sqrt{a^2-\rho_0^2}\left(\frac{\rho_0 e^{i\phi_0}}{4\bar{q}_0\,\bar{s}_0^3}-\frac{1}{2\bar{q}_0^2\bar{s}_0}\right)\end{aligned} \tag{3.20}$$

Finally, the following information for computing the T-stress components can be obtained:

$$\lim_{r\to 0}\sqrt{r}\frac{\partial}{\partial r}\sqrt{r}\sigma_1(z=0)=0 \tag{3.21}$$

$$\lim_{r\Rightarrow 0}\sqrt{r}\,\frac{\partial}{\partial r}\sqrt{r}\sigma_2(z=0)=\Gamma\pi\sqrt{a^2-\rho_0^2}\left(\frac{\rho_0 e^{i\phi_0}}{4\overline{q}_0\ \overline{s}_0^3}-\frac{1}{2\overline{q}_0^2\overline{s}_0}\right) \tag{3.22}$$

By employing the formula (3.3)-(3.5), the T-stress components at any point $(a,\phi,0)$ along the crack front of a penny-shaped crack subjected to a pair of unit normal concentrated forces acting at $(\rho_0,\phi_0,0^{\pm})$ can be related to the stress components in the cylindrical coordinate system $\{\mathbf{0};\rho,\phi,z\}$ defined in section 2.1 by

$$T_{11}^n(\phi;\rho_0,\phi_0)=2\lim_{r\to 0}\sqrt{r}\,\frac{\partial}{\partial r}\sqrt{r}\sigma_{\rho\rho}^n(z=0) \tag{3.23}$$

$$T_{33}^n(\phi;\rho_0,\phi_0)=2\lim_{r\to 0}\sqrt{r}\,\frac{\partial}{\partial r}\sqrt{r}\sigma_{\phi\phi}^n(z=0) \tag{3.24}$$

$$T_{13}^n(\phi;\rho_0,\phi_0)=2\lim_{r\to 0}\sqrt{r}\,\frac{\partial}{\partial r}\sqrt{r}\sigma_{\rho\phi}^n(z=0) \tag{3.25}$$

From the relations (2.7a) and (2.7b) and the results (3.21) and (3.22), the T-stress Green's function becomes

$$T_{11}^n(\phi;\rho_0,\phi_0)=\mathrm{Re}\left\{\Gamma\frac{\pi\sqrt{a^2-\rho_0^2}}{2\sqrt{a}}\left(\frac{\rho_0 e^{i(\phi_0-\phi)}}{2a\left(a-\rho_0 e^{-i(\phi_0-\phi)}\right)\left(a-\rho_0 e^{-i(\phi-\phi_0)}\right)^{3/2}}-\frac{1}{\left(a-\rho_0 e^{-i(\phi_0-\phi)}\right)^2\left(a-\rho_0 e^{-i(\phi-\phi_0)}\right)^{1/2}}\right)\right\} \tag{3.26}$$

$$T_{33}^n(\phi;\rho_0,\phi_0)=-\mathrm{Re}\left\{\Gamma\frac{\pi\sqrt{a^2-\rho_0^2}}{2\sqrt{a}}\left(\frac{\rho_0 e^{i(\phi_0-\phi)}}{2a\left(a-\rho_0 e^{-i(\phi_0-\phi)}\right)\left(a-\rho_0 e^{-i(\phi-\phi_0)}\right)^{3/2}}-\frac{1}{\left(a-\rho_0 e^{-i(\phi_0-\phi)}\right)^2\left(a-\rho_0 e^{-i(\phi-\phi_0)}\right)^{1/2}}\right)\right\} \tag{3.27}$$

$$T_{13}^n(\phi;\rho_0,\phi_0)=\mathrm{Im}\left\{\Gamma\frac{\pi\sqrt{a^2-\rho_0^2}}{2\sqrt{a}}\left(\frac{\rho_0 e^{i(\phi_0-\phi)}}{2a\left(a-\rho_0 e^{-i(\phi_0-\phi)}\right)\left(a-\rho_0 e^{-i(\phi-\phi_0)}\right)^{3/2}}-\frac{1}{\left(a-\rho_0 e^{-i(\phi_0-\phi)}\right)^2\left(a-\rho_0 e^{-i(\phi-\phi_0)}\right)^{1/2}}\right)\right\} \tag{3.28}$$

where $\mathrm{Im}\{f\}$ denotes the imaginary part of the complex function f. It is obvious that the derived Green's function for the T-stress components is singular when $\phi_0 = \phi$ and $\rho_0 = a$. To investigate the order of the present singularity, following variable transformation are introduced:

$$\rho_0 \sin(\phi_0 - \phi) = \bar{r} \sin\bar{\theta} \tag{3.29}$$

$$\rho_0 \cos(\phi_0 - \phi) + \bar{r} \cos\bar{\theta} = a \tag{3.30}$$

where the new variables $\bar{r}$ and $\bar{\theta}$ have the physical interpretation as illustrated in Figure 3.2. Upon the transformations (3.29) and (3.30), the Green's function for the T-stress becomes

$$T_{11}^n(\phi;\rho_0,\phi_0) = \hat{T}_{11}^n(\phi;\bar{r},\bar{\theta}) = \Gamma\frac{\pi}{2}\sqrt{2\cos\bar{\theta}-\frac{\bar{r}}{a}}\left\{\left(\frac{1}{2}-\frac{\bar{r}}{2a}\right)\cos\frac{\bar{\theta}}{2}-\cos\frac{3\bar{\theta}}{2}\right\}\frac{1}{\bar{r}^2} \tag{3.31}$$

$$T_{33}^n(\phi;\rho_0,\phi_0) = \hat{T}_{33}^n(\phi;\bar{r},\bar{\theta}) = -\Gamma\frac{\pi}{2}\sqrt{2\cos\bar{\theta}-\frac{\bar{r}}{a}}\left\{\left(\frac{1}{2}-\frac{\bar{r}}{2a}\right)\cos\frac{\bar{\theta}}{2}-\cos\frac{3\bar{\theta}}{2}\right\}\frac{1}{\bar{r}^2} \tag{3.32}$$

$$T_{13}^n(\phi;\rho_0,\phi_0) = \hat{T}_{13}^n(\phi;\bar{r},\bar{\theta}) = \Gamma\frac{\pi}{2}\sqrt{2\cos\bar{\theta}-\frac{\bar{r}}{a}}\left\{\left(\frac{1}{2}+\frac{\bar{r}}{2a}\right)\sin\frac{\bar{\theta}}{2}+\sin\frac{3\bar{\theta}}{2}\right\}\frac{1}{\bar{r}^2} \tag{3.33}$$

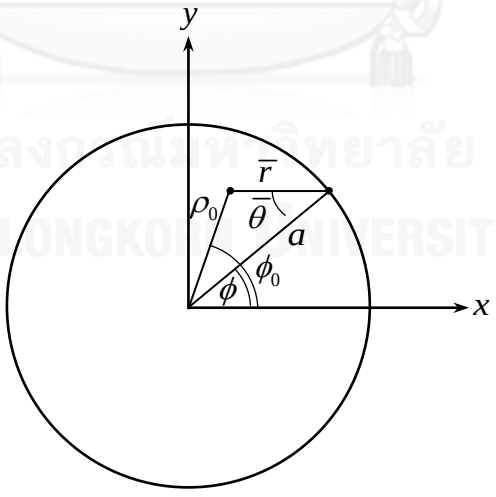

Figure 3.2: Schematic indicating the physical interpretation of variables $\bar{r}$ and $\bar{\theta}$

It is evident from (3.31)-(3.33) that the T-stress Green's functions are dependent on material properties only through the constant Γ and singular only at $\bar{r}=0$ of order $\mathcal{O}(1/\bar{r}^2)$. For the special case of isotropic materials, it can be shown using the appropriate limit process via L'Hôpital rule that

$$\Gamma = -\frac{1-2\nu}{\pi^2} \tag{3.34}$$

3.4 T-stress Green's function for a pair of unit tangential point forces

By applying the same procedure as that utilized in section 3.3, the T-stress Green's function for a penny-shaped crack subjected to a pair of self-equilibrated, unit tangential concentrated forces applied anti-symmetrically to the crack surface can be obtained from the formula (3.3)-(3.5) and the available stress field (2.10). The final results indicate that all components of the T-stress Green's function vanishes, i.e.

$$T_{11}^t(\phi;\rho_0,\phi_0)=0 \tag{3.35}$$

$$T_{33}^t(\phi;\rho_0,\phi_0)=0 \tag{3.36}$$

$$T_{13}^t(\phi;\rho_0,\phi_0)=0 \tag{3.37}$$

It is important to remark that the final trivial results for the T-stress Green's function (3.35)-(3.37) for this particular fundamental loading condition stem directly from the anti-symmetrical feature of the problem. Clearly, the displacement u_x and u_y and the normal stress component σ_{zz} identically vanishes on the plane $z=0$ and this, as a consequence, implies that the normal and shear stresses $\sigma_{\rho\rho}$, $\sigma_{\phi\phi}$ and $\sigma_{\rho\phi}$ also vanish on the plane $z=0$.

3.5 Integral formula for T-stress for arbitrarily applied traction

Finally, let us now consider a penny-shaped crack subjected to arbitrarily distributed, self-equilibrated traction $\boldsymbol{t}^0=\boldsymbol{t}^0(\rho_0,\phi_0)$ as described in Section 2.1. Components of $\boldsymbol{t}^0$ in the x-, y-, and z-directions are denoted by $t_x^0=t_x^0(\rho_0,\phi_0)$, $t_y^0=t_y^0(\rho_0,\phi_0)$, and $t_z^0=t_z^0(\rho_0,\phi_0)$, respectively. By using the linearity of the boundary value problem, the T-stresses for this general loading condition can readily be obtained from the method of superposition along with the results of T-stress Green's functions

(3.31)-(3.33) and (3.35)-(3.37). Final results are expressed in terms of integrals over the crack surface by

$$T_{11}(\phi;\boldsymbol{t}^0)=\int_{-\pi}^{\pi}\int_{0}^{a}T_{11}^{n}(\phi;\rho_0,\phi_0)t_z(\rho_0,\phi_0)\rho_0 d\rho_0 d\phi \tag{3.38}$$

$$T_{33}(\phi;\boldsymbol{t}^0)=\int_{-\pi}^{\pi}\int_{0}^{a}T_{33}^{n}(\phi;\rho_0,\phi_0)t_z(\rho_0,\phi_0)\rho_0 d\rho_0 d\phi \tag{3.39}$$

$$T_{13}(\phi;\boldsymbol{t}^0)=\int_{-\pi}^{\pi}\int_{0}^{a}T_{13}^{n}(\phi;\rho_0,\phi_0)t_z(\rho_0,\phi_0)\rho_0 d\rho_0 d\phi \tag{3.40}$$

By using the transformations (3.29) and (3.30), the integral relations (3.38)-(3.40) becomes

$$T_{11}(\phi;\boldsymbol{t}^0)=\int_{-\pi/2}^{\pi/2}\int_{0}^{2a\cos\bar{\theta}}\hat{T}_{11}^{n}(\phi;\bar{r},\bar{\theta})t_z(\rho_0(\bar{r},\bar{\theta}),\phi_0(\bar{r},\bar{\theta}))\bar{r}d\bar{r}d\bar{\theta} \tag{3.41}$$

$$T_{33}(\phi;\boldsymbol{t}^0)=\int_{-\pi/2}^{\pi/2}\int_{0}^{2a\cos\bar{\theta}}\hat{T}_{33}^{n}(\phi;\bar{r},\bar{\theta})t_z(\rho_0(\bar{r},\bar{\theta}),\phi_0(\bar{r},\bar{\theta}))\bar{r}d\bar{r}d\bar{\theta} \tag{3.42}$$

$$T_{13}(\phi;\boldsymbol{t}^0)=\int_{-\pi/2}^{\pi/2}\int_{0}^{2a\cos\bar{\theta}}\hat{T}_{11}^{n}(\phi;\bar{r},\bar{\theta})t_z(\rho_0(\bar{r},\bar{\theta}),\phi_0(\bar{r},\bar{\theta}))\bar{r}d\bar{r}d\bar{\theta} \tag{3.43}$$

It should be remarked that the integral formula (3.41)-(3.43) involve only the normal component of the applied traction and the integrand is singular at $\bar{r}=0$ of order $\mathcal{O}(1/\bar{r})$. The strong singularity of the integrand requires the integrals to be interpreted in the Cauchy principal sense. It is also important to emphasize that the integral formula (3.41)-(3.43) are applicable only to the traction with its normal component to the crack surface vanish identically along the crack front. This limitation results directly from the development of the T-stress Green's function.

3.6 Numerical evaluation of strongly singular integral

To compute the T-stress of a penny-shaped crack under arbitrarily distributed, self-equilibrated normal traction, it still requires the numerical evaluation of the singular integrals (3.41)-(3.43). It is evident from the T-stress Green's function (3.31)-(3.33) that all involved integrals is of the form

$$I=\int_{-\pi/2}^{\pi/2}\int_{0}^{R(\bar{\theta})}\frac{f(\bar{r},\bar{\theta})}{\bar{r}}d\bar{r}d\bar{\theta} \tag{3.44}$$

where $R(\theta)=2a\cos\theta$ and $f(\bar{r},\bar{\theta})$ is a regular function depending on the applied normal traction and information of the T-stress Green's function. By invoking the condition $t_z(\rho_0(\bar{r}=0,\bar{\theta}),\phi_0(\bar{r}=0,\bar{\theta}))=0$, it is apparent that the function f satisfies the condition

$$\int_{-\pi/2}^{\pi/2} f(0,\bar{\theta})d\bar{\theta}=0 \tag{3.45}$$

From extensive numerical experiments, the numerical integration of the strongly singular integral of the type (3.44) using standard Gaussian quadrature always yields diverged results. To overcome this difficulty, the technique proposed by Cimoroni (1997) is adopted and briefly summarized below. First, the integral (3.44) is decomposed into two parts given by

$$I=\int_{-\pi/2}^{\pi/2}\int_{0}^{R(\bar{\theta})}\frac{f(\bar{r},\bar{\theta})-f(0,\bar{\theta})}{\bar{r}}d\bar{r}d\bar{\theta}+\int_{-\pi/2}^{\pi/2}\int_{0}^{R(\bar{\theta})}\frac{f(0,\bar{\theta})}{\bar{r}}d\bar{r}d\bar{\theta} \tag{3.46}$$

The second integral can be integrated analytically using the Cauchy principal sense along with the condition (3.45) as follows:

$$\begin{aligned}\int_{-\pi/2}^{\pi/2}\int_{0}^{R(\bar{\theta})}\frac{f(0,\bar{\theta})}{\bar{r}}d\bar{r}d\bar{\theta}&=\lim_{\varepsilon\to0^+}\int_{-\pi/2}^{\pi/2}f(0,\bar{\theta})\int_{\varepsilon}^{R(\bar{\theta})}\frac{1}{\bar{r}}d\bar{r}d\bar{\theta}\\&=\lim_{\varepsilon\to0^+}\int_{-\pi/2}^{\pi/2}f(0,\bar{\theta})\left(\ln R(\bar{\theta})-\ln\varepsilon\right)d\bar{\theta}\\&=\int_{-\pi/2}^{\pi/2}f(0,\bar{\theta})\ln R(\bar{\theta})d\bar{\theta}-\left(\lim_{\varepsilon\to0^+}\ln\varepsilon\right)\int_{-\pi/2}^{\pi/2}f(0,\bar{\theta})d\bar{\theta}\\&=\int_{-\pi/2}^{\pi/2}f(0,\bar{\theta})\ln R(\bar{\theta})d\bar{\theta}\end{aligned} \tag{3.47}$$

Now, the integral I becomes

$$I=\int_{-\pi/2}^{\pi/2}\int_{0}^{R(\bar{\theta})}\frac{f(\bar{r},\bar{\theta})-f(0,\bar{\theta})}{\bar{r}}d\bar{r}d\bar{\theta}+\int_{-\pi/2}^{\pi/2}f(0,\bar{\theta})\ln R(\bar{\theta})d\bar{\theta} \tag{3.48}$$

Since the function $f(\bar{r},\bar{\theta})$ is regular, it can be concluded from the Taylor series expansion that $f(\bar{r},\bar{\theta})-f(0,\bar{\theta})=\mathcal{O}(\bar{r})$. In addition, the function $\ln R(\bar{\theta})$ is only weakly singular when $R(\bar{\theta})=0$. As a result, the integral (3.48) can be interpreted in

the sense of Riemann and accurately and efficiently integrated by the standard Gaussian quadrature.

CHAPTER IV
NUMERICAL RESULTS

An extensive numerical study has been conducted for various scenarios and a selected set of results is reported in this chapter to demonstrate both the convergence of the implemented numerical quadrature and the validity of the derived T-stress Green's function and the T-stress integral formula for a penny-shaped crack under general applied tractions by comparing with available benchmark solutions. After the proposed solution and technique are fully tested, the influence of loading regions, load distribution, and material properties on the value and distribution of the T-stress along the crack front is fully investigated.

In the analysis, both isotropic and transversely isotropic material models are considered. For the isotropic case, the Young's modulus E and Poisson's ratio ν are chosen to completely describe its behavior whereas, for the transversely isotropic case, five standard independent material constants utilized are associated with the following constitutive relations (e.g., Staab, 1999 and Singh, 2007)

$$\varepsilon_{xx} = \frac{1}{E_p}\sigma_{xx} - \frac{\nu_p}{E_p}\sigma_{yy} - \frac{\nu_{zp}}{E_z}\sigma_{zz} \tag{4.1}$$

$$\varepsilon_{yy} = -\frac{\nu_p}{E_p}\sigma_{xx} + \frac{1}{E_p}\sigma_{yy} - \frac{\nu_{zp}}{E_z}\sigma_{zz} \tag{4.2}$$

$$\varepsilon_{zz} = -\frac{\nu_{pz}}{E_p}\sigma_{xx} - \frac{\nu_{pz}}{E_p}\sigma_{yy} + \frac{1}{E_z}\sigma_{zz} \tag{4.3}$$

$$\varepsilon_{xy} = \frac{2(1+\nu_p)}{E_p}\sigma_{xy} \tag{4.4}$$

$$\varepsilon_{yz} = \frac{1}{G_{zp}}\sigma_{yz} \tag{4.5}$$

$$\varepsilon_{xz} = \frac{1}{G_{zp}}\sigma_{xz} \tag{4.6}$$

where E_p and ν_p represents the Young's modulus and Poisson's ratio in the isotropic plane, respectively; E_z, G_{zp}, and ν_{zp} denote the out-of-plane Young's modulus, shear modulus and Poisson's ratio, respectively; and ν_{pz} is dependent on

ν_{zp} via the relation $\nu_{zp}/E_z = \nu_{pz}/E_p$. While the key results obtained in the present study are derived in terms of different material constants A_{11}, A_{13}, A_{33}, A_{44} and A_{66}, these two different sets of material parameters are equivalent and can be related by using the constitutive relations (2.3) and (4.1)-(4.6).

4.1 Verification

As an example for testing the numerical quadrature and verifying the derived results, let us consider a penny-shaped crack subjected to two load cases: (i) a uniformly distributed normal traction σ_0 acting to the crack over a circular region of radius a_0, $a_0 < a$ and centered at the origin as shown in Figure 4.1(a) and (ii) a linearly distributed normal traction $\sigma_0(1+x/a_0)/2$ acting to the crack over a circular region of radius a_0, $a_0 < a$ and centered at the origin as shown in Figure 4.1(b). These two scenarios are chosen as a representative of axisymmetric and non-axisymmetric loads, respectively. In the analysis, the loading region $a_0 = 0.5a$, the Poisson's ratio $\nu = 0.3$ and Young's modulus $E = 1MPa$ for the isotropic case, and $A_{11} = 126GPa$, $A_{13} = 53GPa$, $A_{33} = 117GPa$, $A_{44} = 35.3GPa$ and $A_{66} = 35.5GPa$ for the transversely isotropic case are utilized.

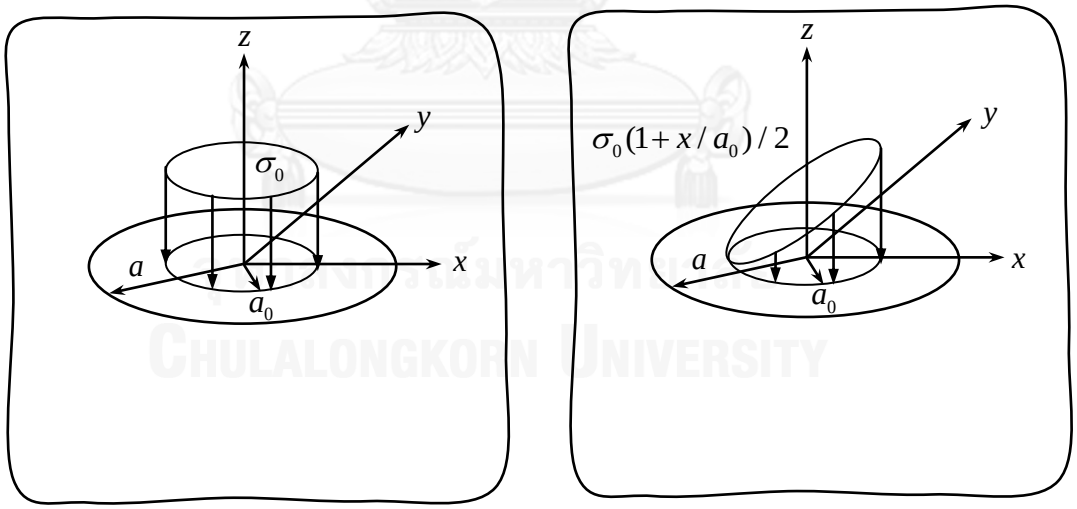

(a) (b)

Figure 4.1 (a) Penny-shaped crack subjected to uniformly distributed normal traction σ_0 over a circular region of radius a_0, $a_0 < a$ and centered at the origin and (b) Penny-shaped crack subjected to linearly distributed normal traction $\sigma_0(1+x/a_0)/2$ over a circular region of radius a_0, $a_0 < a$ and centered at the origin

To evaluate the integral of the type (3.48) numerically, the ranges of the integration in the $\bar{r}$ - and $\bar{\theta}$ -directions are subdivided into N_r and N_θ intervals and, for each interval, the number of integration points employed is denoted by N_i. The accuracy of the numerical integration can be controlled by N_r, N_θ, and N_i. Numerical results obtained for various values of N_r, N_θ, and N_i are compared with the benchmark solution (obtained by setting $N_r = N_\theta = 20$ and $N_i = 50$) and reported in Table 4.1 for the first loading case and in Tables 4.2 and 4.3 for the second loading case. It is remarked that the benchmark solution used in the comparison is generated by using sufficiently large N_r, N_θ, and N_i to ensure that it represents the converged value of the integral. Note in addition that for the non-axisymmetric case, results shown in the table are associated with the maximum T-stress. It is obviously seen that convergence of the calculated T-stress depends significantly on the number of integration points, number of sub-intervals, and loading conditions but clearly independent of the material properties. The latter observation results directly from the fact that the material properties affect only the constant Γ. As anticipated, as N_r, N_θ, and N_i increase, the computed results converge nicely to the reference solution.

Table 4.1: Percent error of T-stress compared with reference solution for penny-shaped crack subjected uniformly distributed normal traction with $a_0 = 0.5a$

		$\lvert(T_{11} - T_{11}^{ref})/T_{11}^{ref}\rvert \times 100$ or $\lvert(T_{33} - T_{33}^{ref})/T_{33}^{ref}\rvert \times 100$	
N_i	$N_r,\ N_\theta$	**Isotropic case**	**Transversely isotropic case**
5	1	0.2098	0.2098
	3	0.0418	0.0418
	5	0.0196	0.0196
	10	0.0069	0.0069
	20	0.0025	0.0025
	50	0.0006	0.0006
10	1	0.0309	0.0309
	3	0.0060	0.0060
	5	0.0028	0.0028
	10	0.0010	0.0010
	20	0.0003	0.0003
	50	0.0001	0.0001

Table 4.2: Percent error of maximum T-stress T_{11} or T_{33} compared with reference solution for penny-shaped crack under linear normal traction with $a_0 = 0.5a$

		$\lvert (T_{11,\max} - T_{11,\max}^{ref}) / T_{11,\max}^{ref} \rvert \times 100$ or $\lvert (T_{33,\max} - T_{33,\max}^{ref}) / T_{33,\max}^{ref} \rvert \times 100$	
N_i	N_r, N_θ	Isotropic case	Transversely isotropic case
5	1	0.2575	0.2575
	3	0.0506	0.0506
	5	0.0236	0.0236
	10	0.0083	0.0083
	20	0.0029	0.0029
	50	0.0007	0.0007
10	1	0.0374	0.0374
	3	0.0072	0.0072
	5	0.0033	0.0033
	10	0.0012	0.0012
	20	0.0004	0.0004
	50	0.0001	0.0001

Table 4.3: Percent error of maximum T-stress T_{13} compared with reference solution for penny-shaped crack under linear normal traction with $a_0 = 0.5a$

		$\lvert (T_{13,\max} - T_{13,\max}^{ref}) / T_{13,\max}^{ref} \rvert \times 100$	
N_i	N_r, N_θ	Isotropic case	Transversely isotropic case
5	1	1.2436	1.2436
	3	0.2252	0.2252
	5	0.1033	0.1033
	10	0.0361	0.0361
	20	0.0127	0.0127
	50	0.0032	0.0032
10	1	0.1648	0.1648
	3	0.0311	0.0311
	5	0.0144	0.0144
	10	0.0050	0.0050
	20	0.0017	0.0017
	50	0.0004	0.0004

For all results presented further below, $N_r = N_\theta = 5$ and $N_i = 5$ are chosen in the analysis. The discrepancy between the computed T-stresses and the converged solution is expected to be less than 0.10%.

To verify the derived T-stress Green function and the implementation to treat arbitrarily applied normal traction, the proposed solutions for both loading cases shown in Figure 4.1 are compared with the benchmark results generated by a numerical technique introduced by Subsathaphol *et al.* (2014). For a penny-shaped crack subjected to a uniformly distributed normal traction, the normalized non-zero T-stress components for both isotropic and transversely isotropic cases are reported in Table 4.3. It can be seen from this set of results that the T-stress components generated by the proposed integral formula show excellent agreement with the benchmark solution with the discrepancy less than 1% for both material models. For the second loading case, all T-stress components exist and they vary along the crack front. The computed T-stresses normalized by σ_0 are reported, as a function of the angular position θ measured from the x-axis, in Figure 4.2 for the isotropic case and in Figure 4.3 for the transversely isotropic case. Again, it can be concluded for this particular loading condition that the analytical solution obtained in the present study is nearly identical to that obtained from the numerical technique for isotropic and transversely isotropic cases. Unlike the axisymmetric load considered in the previous case, the T-stress component T_{13} does not vanish along the crack front but its magnitude is less than that of T_{11} and T_{33}. In addition, the values of the T-stress shown are nearly identical for both material models.

Table 4.4: Normalized non-zero T-stress of penny-shaped crack subjected to uniformly distributed normal traction with $a_0 = 0.5a$. Results are compared with benchmark solution generated by technique proposed by Subsathaphol *et al.* (2014).

	Isotropic case			Transversely isotropic case		
T-stress	Current sol.	Ref. sol.	% diff	Current sol.	Ref. sol.	% diff
T_{11}/σ_0	0.0500	0.0505	0.99%	0.0509	0.0513	0.79
T_{33}/σ_0	-0.0500	-0.0499	0.20%	-0.0509	-0.0507	0.39

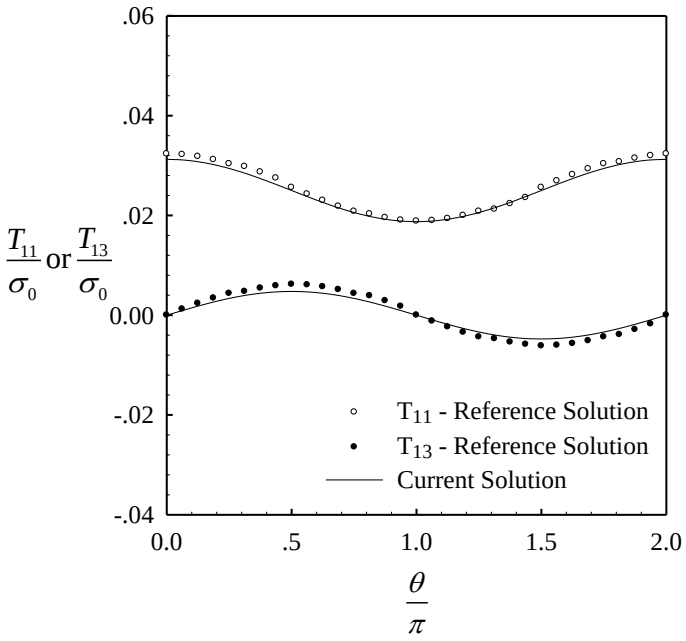

Figure 4.2 Normalized T-stress components for penny-shaped crack subjected to linearly distributed normal traction with $a_0 = 0.5a$. Results are reported for isotropic case.

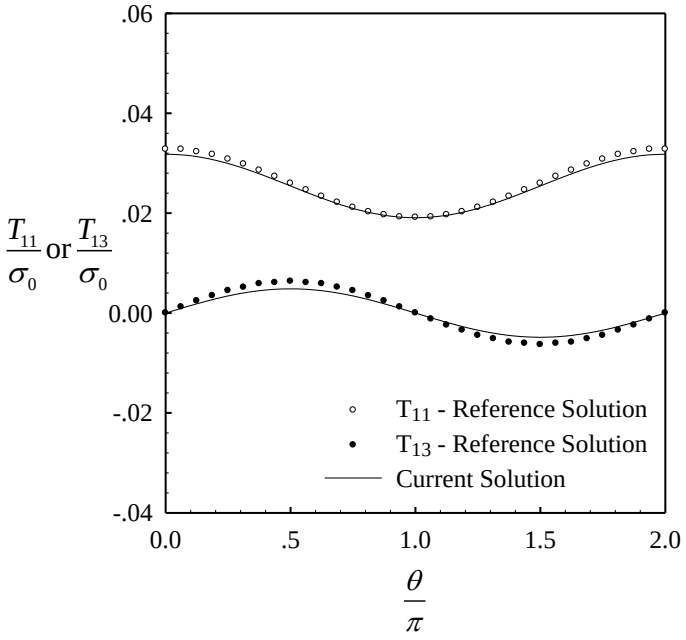

Figure 4.3 Normalized T-stress components for penny-shaped crack subjected to linearly distributed normal traction with $a_0 = 0.5a$. Results are reported for transversely isotropic case

4.2 Behavior of T-stress Green's function

In this particular section, the behavior of the derived T-stress Green's function including the dependence on material properties, dependence on the applied load location, and the variation along the crack front are briefly explored.

It should be evident from the explicit formula (3.31)-(3.33) and (3.17) that the T-stress Green's function T_{11}^n, T_{33}^n and T_{13}^n are dependent on the material properties only through the constant parameter Γ. Since all T-stress components are linear with respect to Γ, the influence of the material properties on their values and distribution along the crack front can be completely described by the material-dependent characteristic of Γ. For the special case of isotropy, the constant Γ depends linearly on the Poisson's ratio but independent of the Young's modulus via the relation (3.34). The plot of Γ for the whole applicable range of ν is shown in Figure 4.4. It can be seen that as the Poisson's ratio increases, the magnitude of Γ decreases and, as a result, the T-stress Green's function also decreases in magnitude. In addition, Γ and the T-stress Green's function vanish for the incompressible material with $\nu = 0.5$. For transversely isotropic case, Γ is found to depend only on the ratio of the material constants and, in the present study, the dependence on ν_p, ν_{pz}, E_p/E_z, and G_{zp}/E_z are investigated. To obtain the variation of Γ with respect to each parameter, a following strategy is employed: (i) the elastic constants of a particular material (chosen to be the same as those used in section 4.1) are converted to ν_p, ν_{pz}, E_p, E_z and G_{zp}, (ii) one of the ratios ν_p, ν_{pz}, E_p/E_z, and G_{zp}/E_z is selected and varied while other parameters remains fixed, (iii) a new set of ν_p, ν_{pz}, E_p, E_z and G_{zp} is converted to A_{11}, A_{13}, A_{33}, A_{44} and A_{66}, and (iv) the value of Γ is computed. The variation of Γ with respect to ν_p, ν_{pz}, E_p/E_z, and G_{zp}/E_z are reported in Figures 4.5, 4.6, 4.7, and 4.8, respectively. It should be evident that Γ depends almost linearly on both ν_p and ν_{pz}, depends nonlinearly on the ratio E_p/E_z, and is independent of the ratio G_{zp}/E_z. In particular, as both the Poisson ratios ν_p and ν_{pz} increase, the magnitude of the parameter Γ decreases. The material-dependence characteristics of Γ should provide the sufficient information of the influence of material properties on the T-stress Green's function and also the T-stress for a penny-shaped crack subjected to arbitrarily applied traction. For a parametric study carried out further, two representative material models shown in Section 4.1 are used throughout.

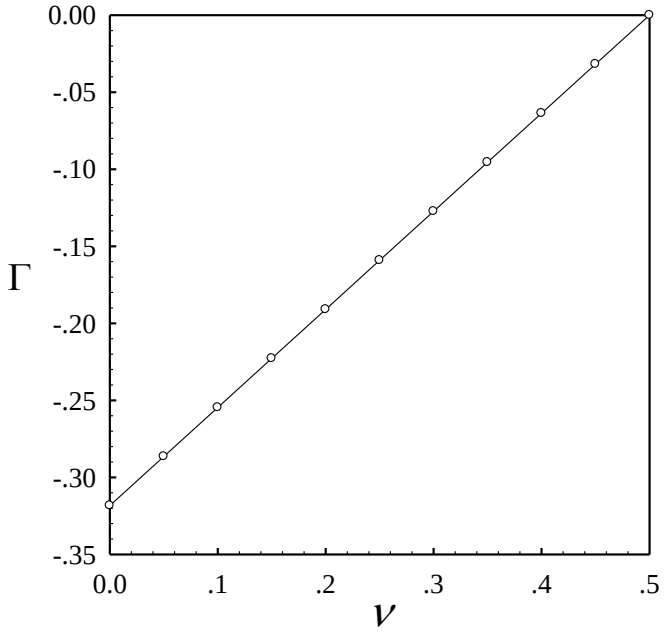

Figure 4.4 Dependence of material parameter Γ on Poisson's ratio ν for isotropic case

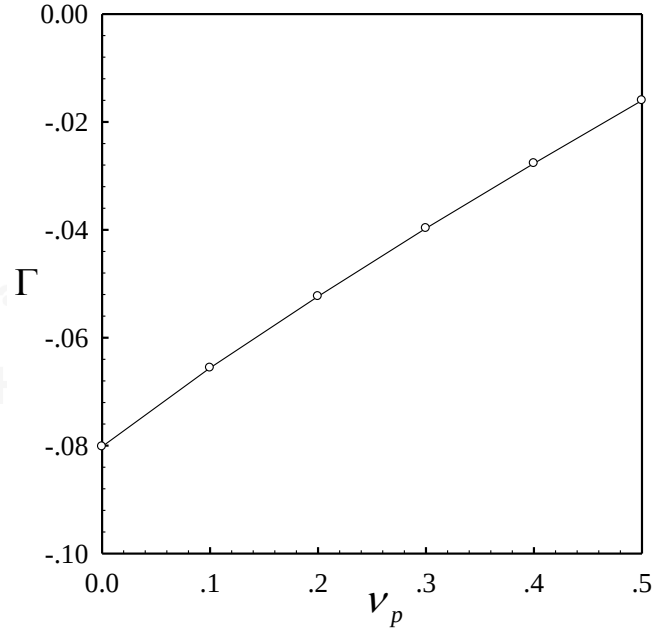

Figure 4.5 Dependence of material parameter Γ on ν_p for transversely isotropic case

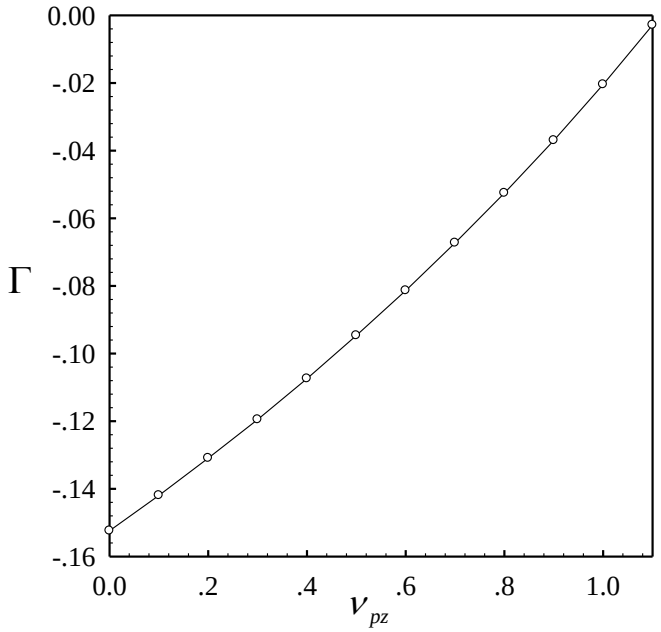

Figure 4.6 Dependence of material parameter Γ on ν_{pz} for transversely isotropic case

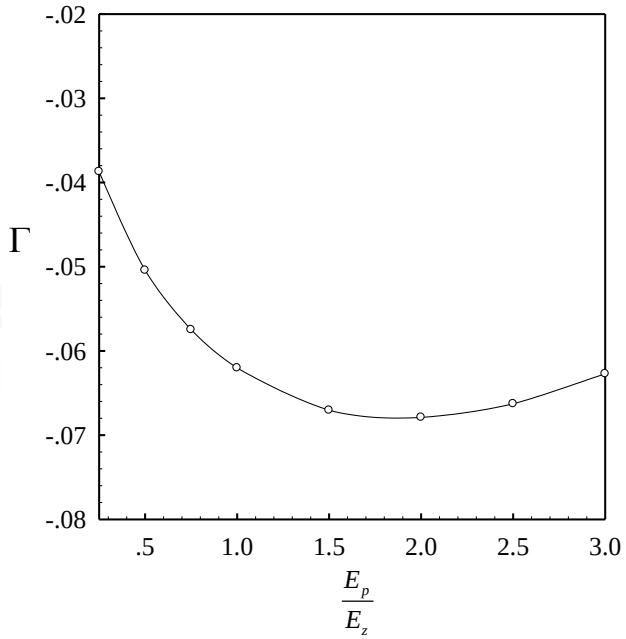

Figure 4.7 Dependence of material parameter Γ on E_p / E_z for transversely isotropic case

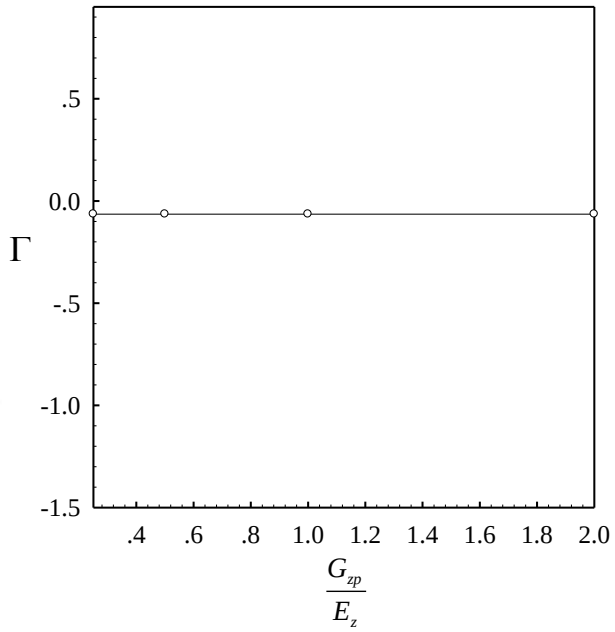

Figure 4.8 Dependence of material parameter Γ on G_{zp}/E_z for transversely isotropic case

The T-stress Green's functions along the crack front for different applied load locations are reported in Figures 4.9 and 4.10 for the isotropic case and Figures 4.11 and 4.12 for the transversely isotropic case. It can be seen that the variation of the T-stress Green's function depend strongly on the location of the applied unit concentrated force; in particular, as the location of the applied force approaches the crack front $\rho_0 \to a$, the value of $T_{11}^n = -T_{33}^n$ and T_{13}^n become infinite at $\phi - \phi_0 = 0$. In addition, the distribution of $T_{11}^n = -T_{33}^n$ and T_{13}^n possesses a symmetric and anti-symmetric feature with respect to the axis $\phi - \phi_0 = 0$, respectively. Results for both representative material models considered are nearly identical since the value of Γ for the isotropic case with $\nu = 0.3$ and the transversely isotropic case with elastic constants and $A_{11} = 126GPa$, $A_{13} = 53GPa$, $A_{33} = 117GPa$, $A_{44} = 35.3GPa$ and $A_{66} = 35.5GPa$ are very close (i.e., $\Gamma = -0.04053$ and $\Gamma = -0.04125$, respectively).

4.3 Influence of Loading Condition

In this section, the influence of the loading region and the distribution of the applied normal traction on the crack surface for both axisymmetric and non-axisymmetric cases on the value and variation of the T-stress along the crack front is investigated.

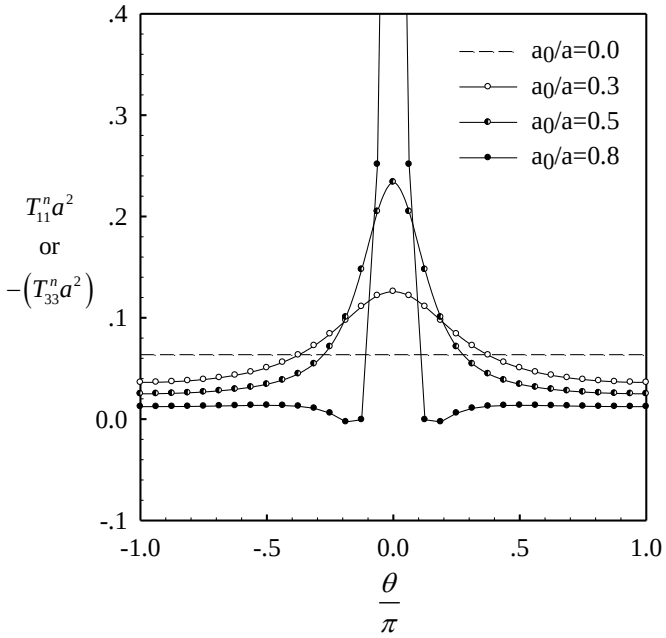

Figure 4.9 Normalized T-stress Green's function $T_{11}^n = -T_{33}^n$ along the crack front for isotropic case

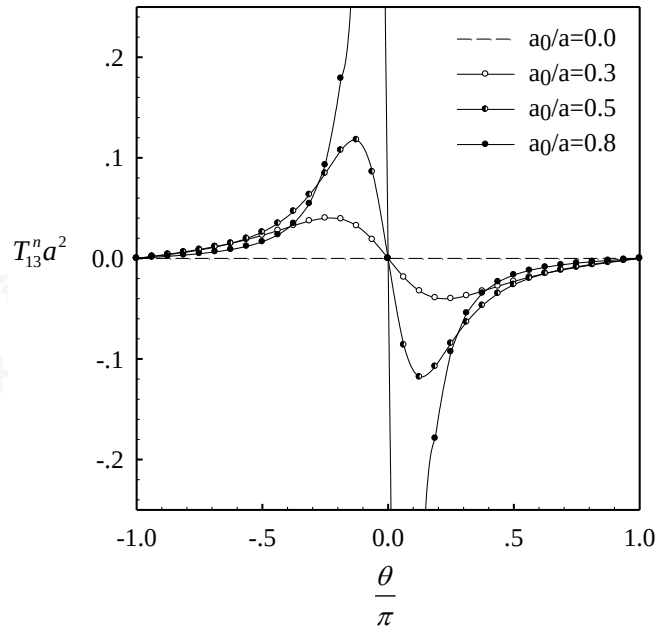

Figure 4.10 Normalized T-stress Green's function T_{13}^n along the crack front for isotropic case

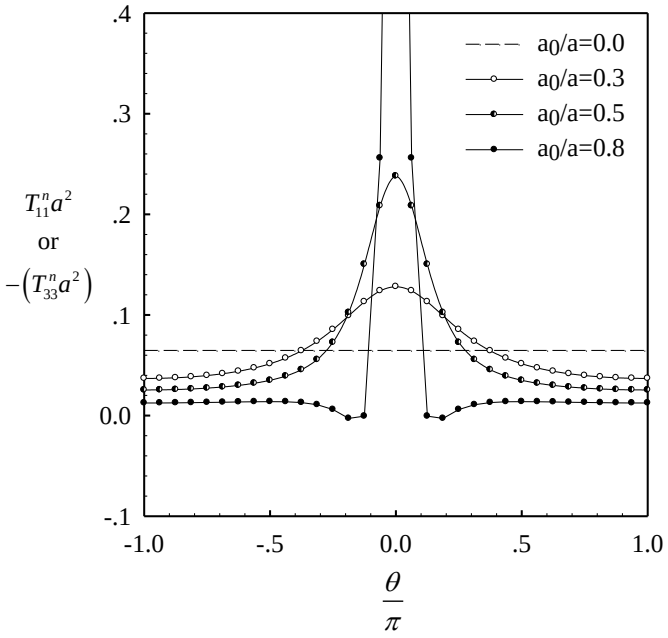

Figure 4.11 Normalized T-stress Green's function $T_{11}^n = -T_{33}^n$ along the crack front for transversely isotropic case

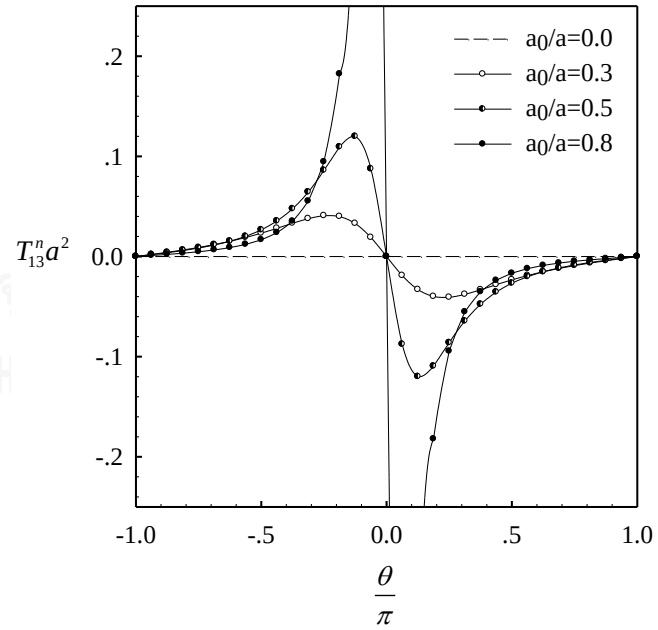

Figure 4.12 Normalized T-stress Green's function T_{13}^n along the crack front for transversely isotropic case

To represent a variety of loading conditions, following six cases of applied normal tractions are investigated: (i) a uniformly distributed normal traction σ_0 over a circular region of radius a_0 with $a_0 < a$ as shown in Figure 4.1(a), (ii) a linearly distributed normal traction $\sigma_0(1-\rho/a_0)$ over a circular region of radius a_0 as shown in Figure 4.13(a), (iii) a parabolic normal traction $\sigma_0(1-(\rho/a_0)^2)$ over a circular region of radius a_0 as shown in Figure 4.13(b); (iv) a linearly distributed normal traction $\sigma_0(1+x/a_0)/2$ over a circular region of radius a_0 with $a_0 < a$ as shown in Figure 4.1(b), (v) a parabolic normal traction $\sigma_0(1+(x/a_0)^2)/2$ over a circular region of radius a_0 with $a_0 < a$ as shown in Figure 4.14(a), and (vi) a cubic normal traction $\sigma_0(1+(x/a_0)^3)/2$ over a circular region of radius a_0 with $a_0 < a$ as shown in Figure 4.14(b). The first three cases are chosen to represent the axisymmetric loading condition whereas the last three correspond to the non-axisymmetric loading condition.

First, the size of the loading region a_0 is investigated. Since the influence of material properties on the T-stress is lumped to the parameter Γ, it is sufficient to perform the parametric study for one selected material model and, here, the transversely isotropic material with elastic constants given in section 4.1 is employed.

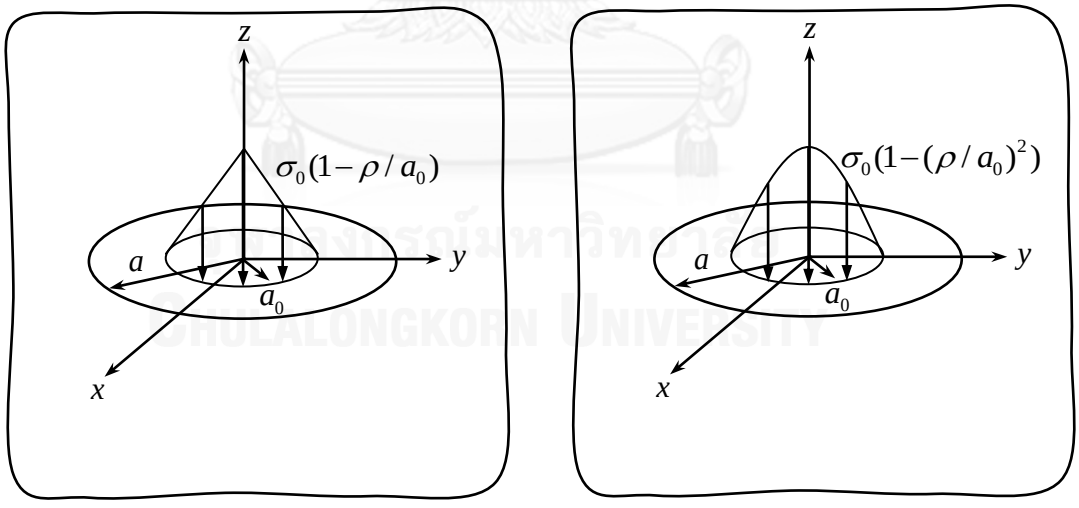

(a) (b)

Figure 4.13 (a) Penny-shaped crack subjected to linearly distributed normal traction $\sigma_0(1-\rho/a_0)$ over a circular region of radius a_0 and (b) Penny-shaped crack subjected to parabolic normal traction $\sigma_0(1-(\rho/a_0)^2)$ over a circular region of radius a_0

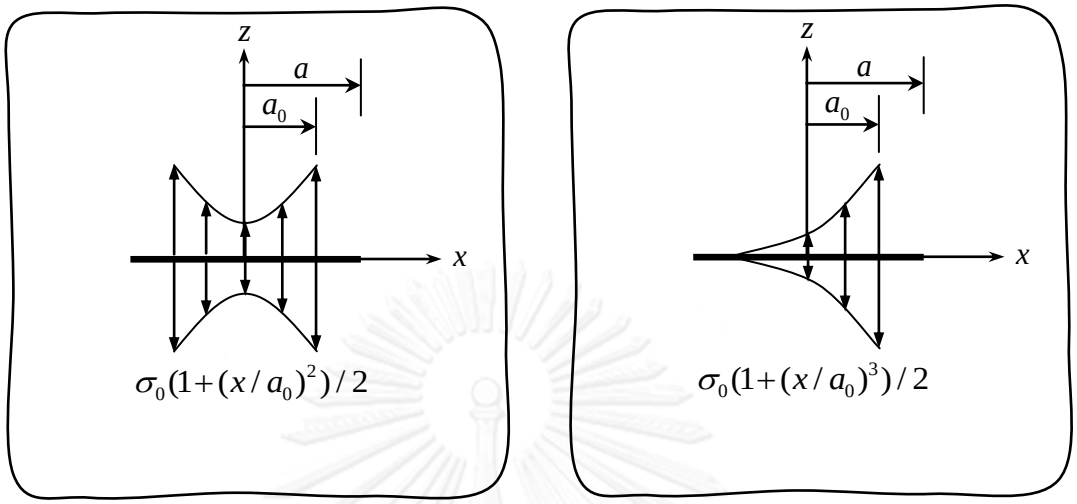

(a) (b)

Figure 4.14 (a) Penny-shaped crack subjected to parabolic normal traction $\sigma_0(1+(x/a_0)^2)/2$ over a circular region of radius a_0 with $a_0 < a$ and (b) penny-shaped crack subjected to cubic normal traction $\sigma_0(1+(x/a_0)^2)/2$ over a circular region of radius a_0 with $a_0 < a$

To allow the comparison for all loading cases, the resultants of all applied tractions are controlled to be the same and denoted by P. For the axisymmetric loading conditions, only T_{11} and T_{33} are non-zero and they are constant along the crack front. The computed non-zero T-stresses for the load case (i), (ii) and (iii) are normalized by P/a^2 and then reported in Table 4.4 for various values of the normalized loading region a_0/a. It is can be concluded from this set of results that, for the axisymmetric case, once the T-stresses are properly normalized by the resultant force P, they are independent of both the normalized loading region a_0/a and the load distribution.

For the non-axisymmetric loading conditions, T_{11}, T_{33} and T_{13} are non-zero and they vary along the crack front. The computed T-stresses normalized by P/a^2 are reported in Figures 4.15 and 4.16 for the load case (iv), Figures 4.17 and 4.18 for the load case (v), and Figures 4.19 and 4.20 for the load case (vi). Results are shown for various values of the normalized loading region a_0/a ranging from 0.1 to 0.9. It can be seen that the T-stress components T_{11} and T_{33} exhibit only slight variation along the crack front for a small loading region a_0/a and, as a_0/a, the variation is

more evident with significant discrepancy between its maximum and minimum values. In addition, the value of T_{11} and $-T_{33}$ remains positive for the entire crack front but the shape of the variation curve depends strongly on the distribution of the applied normal traction. For the T-stress component T_{13}, its value nearly vanishes along the crack front when the size of the loading region a_0/a is relatively small. This is due to the fact that the applied normal traction is close to the concentrated force P applied to the center of the crack ($a_0/a=0$) and, as a result, the detail of the load variation on that small region is insignificant. As the size of the loading region a_0/a increases, the value of T_{13} becomes significant and is the same order of that of T_{11} and $-T_{33}$. Similar to T_{11} and $-T_{33}$, the variation of T_{13} along the crack front are more apparent for a larger a_0/a and the shape of such variation curve depends primarily on the load distribution. In contrast to the case of T_{11} and $-T_{33}$, the T-stress component T_{13} can take either positive or negative value along the crack front.

Table 4.5: Normalized T-stress $T_{11}=-T_{33}$ of penny-shaped crack subjected to load cases (i), (ii) and (iii). Results are reported for transversely isotropic material used in Section 4.1

	$T_{11}a^2/P$ or $-T_{33}a^2/P$		
a_0/a	Load case (i)	Load case (ii)	Load case (iii)
0.1	0.0648	0.0648	0.0648
0.2	0.0648	0.0648	0.0648
0.3	0.0648	0.0648	0.0648
0.4	0.0648	0.0648	0.0648
0.5	0.0648	0.0648	0.0648
0.6	0.0648	0.0648	0.0648
0.7	0.0648	0.0648	0.0648
0.8	0.0648	0.0648	0.0648
0.9	0.0648	0.0648	0.0648
1	-	0.0648	0.0648

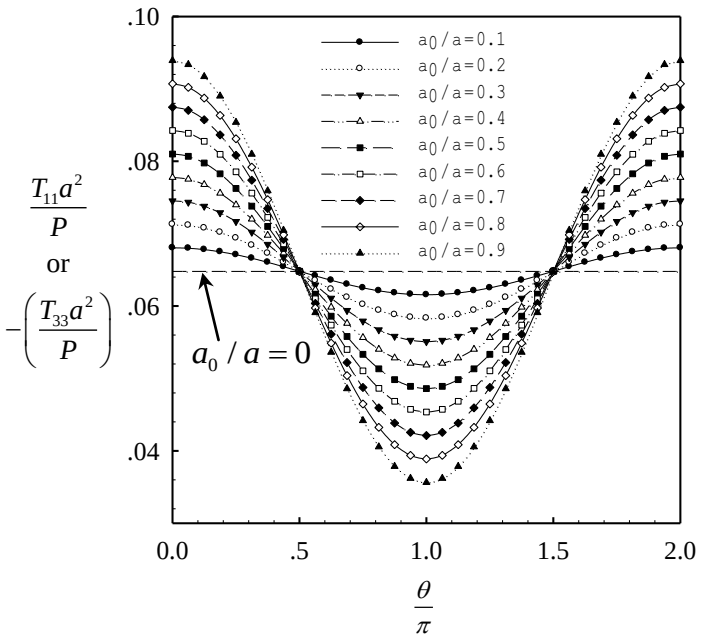

Figure 4.15 Normalized T-stress T_{11} (or $-T_{33}$) along the crack front of penny-shaped crack subjected to load case (iv). Results are reported for transversely isotropic material indicated in Section 4.1.

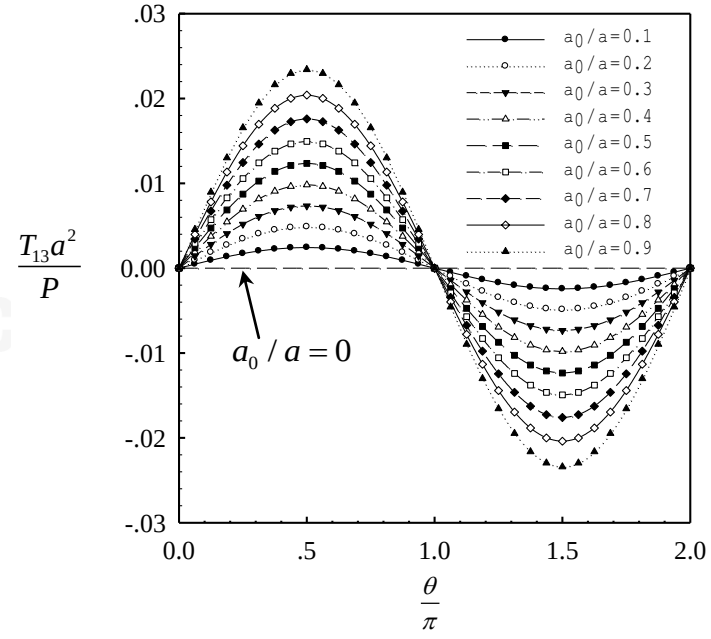

Figure 4.16 Normalized T-stress T_{13} along the crack front of penny-shaped crack subjected to load case (iv). Results are reported for transversely isotropic material indicated in Section 4.1.

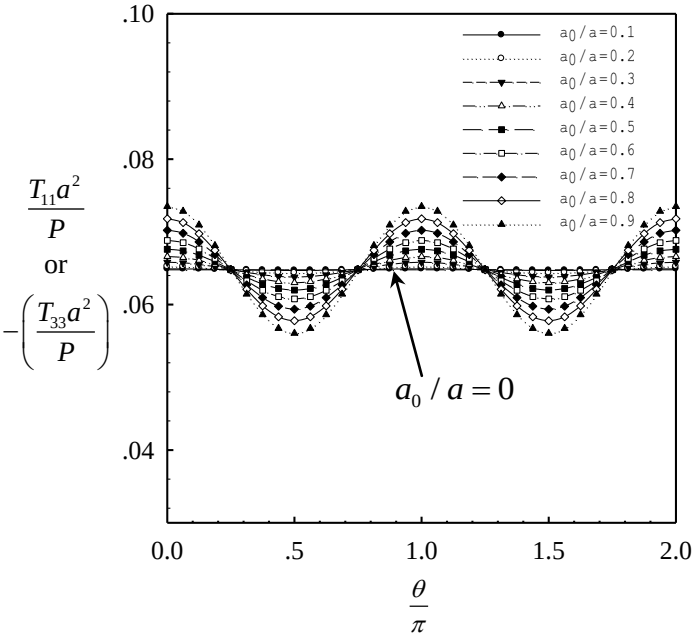

Figure 4.17 Normalized T-stress T_{11} (or $-T_{33}$) along the crack front of penny-shaped crack subjected to load case (v). Results are reported for transversely isotropic material indicated in Section 4.1.

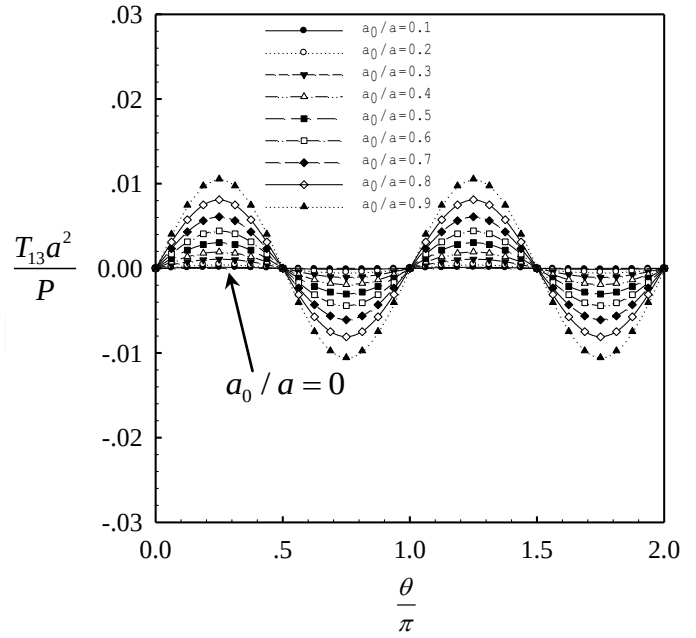

Figure 4.18 Normalized T-stress T_{13} along the crack front of penny-shaped crack subjected to load case (v). Results are reported for transversely isotropic material indicated in Section 4.1.

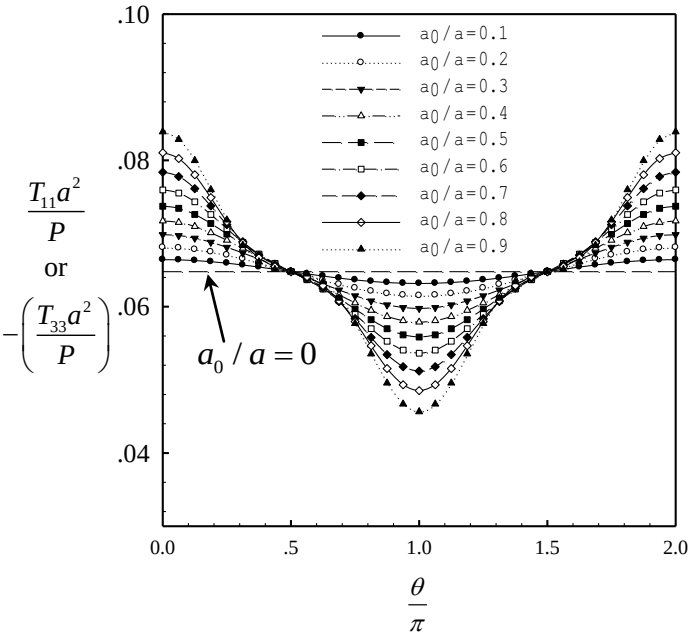

Figure 4.19 Normalized T-stress T_{11} (or $-T_{33}$) along the crack front of penny-shaped crack subjected to load case (vi). Results are reported for transversely isotropic material indicated in Section 4.1.

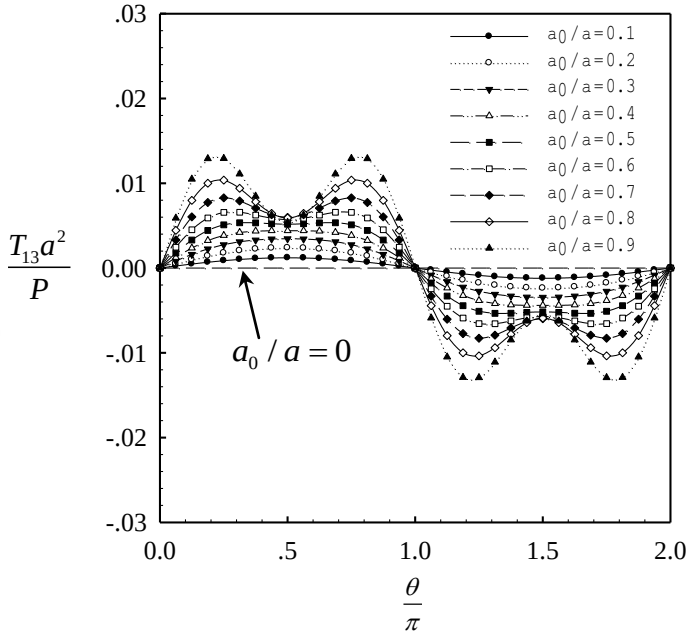

Figure 4.20 Normalized T-stress T_{13} along the crack front of penny-shaped crack subjected to load case (vi). Results are reported for transversely isotropic material indicated in Section 4.1.

CHAPTER V
CONCLUSIONS AND REMARKS

A closed form solution for the T-stress Green function of a penny-shaped crack embedded in a homogeneous, three-dimensional, transversely isotropic, linearly elastic medium subjected to a pair of self-equilibrated unit normal and unit tangential concentrated forces acting to any location on the crack surface has been established. The existing complete stress fields for both fundamental loading conditions derived by a potential-theory-based technique have been used along with the asymptotic representation of the near-tip stress and the proper limiting process to construct the T-stress Green's function. It has been found from the anti-symmetric condition that the T-stress Green's function for the case of applied unit tangential concentrated forces identically vanishes along the crack front and this implies that the component of the applied traction tangent to the plane of the crack plays no role on the value of the T-stress along the crack front.

The method of superposition has been utilized along with the derived T-stress Green's function to establish the integral formula for computing the T-stress of a penny-shaped crack subjected to self-equilibrated, arbitrarily distributed traction. The resulting formula involves strongly singular integral that must be properly interpreted in the Cauchy principal sense. A selected numerical quadrature has been implemented to accurately and efficiently evaluate the Cauchy singular integral. An extensive numerical study has been conducted and confirmed the performance of the implemented numerical integration scheme. A series of numerical results has been generated and compared with available benchmark solutions. It has been found from such numerical experiments that the derived solutions show good agreement with the reference solutions and this should confirm both the derivation of the T-stress Green's function and the implementation of the proposed integral formula.

It has been pointed out that the dependence on the material properties of the derived T-stress Green's function is completely described by a linearly dependent constant parameter Γ. For the special case of an isotropic medium, such parameter has been found independent of the Young's modulus and linear dependent on the Poisson's ratio. As a result, the T-stress Green's function and also the T-stress for any applied traction depend linearly on the Poisson's ratio. In addition, as the value of Poisson's ratio increases to 0.5, the magnitude of the T-

stress decreases to zero. For the transversely isotropic case, an extensive investigation of the material-dependent behavior of the parameter Γ has indicated that it is strongly dependent on the parameters ν_p, ν_{pz} and E_p/E_z but independent of the modulus ratio G_{zp}/E_z. Similar to the isotropic case, the dependence on the two Poisson ratios ν_p and ν_{pz} has been found almost linear and the magnitude of Γ (or T-stress) reduces as ν_p and ν_{pz} increases.

From the in-depth investigation of the influence of loading region and loading distribution, it has been found that only the T-stress components T_{11} and T_{33} are constant along the crack front and independent of the size of the loading region and the loading distribution for the axisymmetric normal traction applied over a concentric circular region provided that the resultants of the applied traction are the same. For non-axisymmetric loads applied over a concentric circular region, the value of the T-stress and its variation along the crack front has been found strongly dependent on both the size of the loading region and the loading distribution. For a small loading region, the T-stresses T_{11} and T_{33} are nearly constant and T_{13} is nearly zero and almost independent of the load distribution since the applied normal traction is approximately close to the normal concentrated force applied at the center of the crack which is asymmetric. For a large loading region, the variation of T_{11}, T_{33} and T_{13} is evident and the shape of the variation curve depends strongly on the load distribution.

As a final remark, the T-stress Green's function developed in the present study has been limited to that the location of the applied concentrated force must not be along the crack front. As a result, the developed integral formula can be applied only to the traction that vanishes identically along the crack front. In addition, the T-stress Green's function has been developed only for a pair of self-equilibrated unit normal and tangential concentrated forces. This also limits the application of the integral formula to treat a penny-shaped crack under non-self-equilibrated tractions. Alleviation of the current limitations is potentially useful and can broaden the capability of the integral formula to treat more practical cases.

REFERENCES

Anderson, T. L. (2005). Fracture Mechanics : Fundamentals and Applications, Third Edition. CRC Press, Boca Raton.

Cimoroni, M. G. (1997). "Numerical evaluation of a 2-D Cauchy principal value integral based on quasi-interpolating splines." Approximation Theory and its Applications 13(4): 1-12.

Du, Z. Z., and Hancock, J. W. (1991). "The effect of non-singular stresses on crack-tip constraint." Journal of the Mechanics and Physics of Solids 39: 555-567.

Fabrikant, V. I. (1989). Applications of Potential Theory in Mechanics. Kluwer Academic Publishers, Netherlands.

Fett, T. (1997). "A Green's function for T-stresses in an edge-cracked rectangular plate." Engineering Fracture Mechanics 57: 365-373.

Fett, T. (1998). "T-stresses in rectangular plates and circular disks." Engineering Fracture Mechanics 60: 631-652.

Fett, T., and Rizzi, G. (2006). "T-stress of cracks loaded by near-tip tractions." Engineering Fracture Mechanics 73(13): 1940-1946.

Fett, T., Rizzi, G., and Bahr, H.-A. (2006). "Green's functions for the T-stress of small kink and fork cracks." Engineering Fracture Mechanics 73(10): 1426-1435.

Kirilyuk, V. S., and Levchuk, O. I. (2007). "Elastic T-stress solutions for flat elliptical cracks under tension and bending." Engineering Fracture Mechanics 74(17): 2881-2891.

Lewis, T., and Wang, X. (2008). "The T-stress solutions for through-wall circumferential cracks in cylinders subjected to general loading conditions." Engineering Fracture Mechanics 75(10): 3206-3225.

Meshii, T., Tanaka, T., and Lu, K. (2010). "T-Stress solutions for a semi-elliptical axial surface crack in a cylinder subjected to mode-I non-uniform stress distributions." Engineering Fracture Mechanics 77(13): 2467-2478.

Molla-Abbasi, K., and Schütte, H. (2008). "On the full set of elastic T-stress terms of internal elliptical cracks under mixed-mode loading condition." Engineering Fracture Mechanics 75(6): 1545-1568.

Qu, J., and Wang, X. (2006). "Solutions of T-stresses for quarter-elliptical corner cracks in finite thickness plates subject to tension and bending." International Journal of Pressure Vessels and Piping 83(8): 593-606.

Rice, J. R. (1974). "Limitations to the small scale yielding approximation for crack tip plasticity." Journal of the Mechanics and Physics of Solids 22: 17-26.

Schütte, H., and Molla-Abbasi, K. (2007). "On the full set of elastic T-stress terms of internal circular cracks under mixed-mode loading conditions." Engineering Fracture Mechanics 74(17): 2770-2787.

Sedighiani, K., Mosayebnejad, J., Ehsasi, H., and Sahraei, H. R. (2011). "The effect of T-stress on the brittle fracture under mixed mode loading." Procedia Engineering 10: 774-779.

Singh, A. K. (2007). Mechanics of Solids. Prentice-Hall of India Private Limited, New Delhi.

Staab, G. H. (1999). Laminar Composites. Butterworth-Heinemann, Boston.

Subsathaphol, T., Rungamornrat, J., and Phongtinnaboot, W. (2014). "ANALYSIS OF T-STRESS FOR CRACKS IN 3D LINEAR PIEZOELECTRIC MEDIA." The 19th National Convention on Civil Engineering 1: 97.

Wang, X. (2002). "Elastic T-stress for cracks in test specimens subjected to non-uniform stress distribution." Engineering Fracture Mechanics 69: 1339–1352.

Wang, X. (2003). "Elastic T-stress solutions for semi-elliptical surface cracks in finite thickness plates." Engineering Fracture Mechanics 70: 731-756.

Wang, X. (2004). "Elastic T-stress solutions for penny-shaped cracks under tension and bending." Engineering Fracture Mechanics 71(16-17): 2283-2298.

Wang, X., and Bell, R. (2004). "Elastic T-stress solutions for semi-elliptical surface cracks in finite thickness plates subject to non-uniform stress distributions." Engineering Fracture Mechanics 71(9-10): 1477-1496.

Williams, M. L. (1957). "On the stress distribution at the base of a stationary crack." ASME Journal of Applied Mechanics 24: 109-114.

Zhou, Z., Xu, X., Leung, A. Y. T., and Huang, Y. (2013). "Stress intensity factors and T-stress for an edge interface crack by symplectic expansion." Engineering Fracture Mechanics 102: 334-347.

VITA

Matana Pinitpanich was born on April 3rd, 1987. He graduated from Suphannapoom and Suankularb Wittayalai school respectively. In 2005, he also entranced to faculty of engineering of Chulalongkorn University in department of Civil Engineering and then graduated his bachelor degree in 2009. After this graduation, in 2011 he continued his Master of Engineering degree in Structural Engineering major. Finally, he decided to do his research in field of Solid Mechanics under the supervision of Associate Professor Dr.Jaroon Rungamornrat.